Model calculation of nucleon structure functions

X. Song* and J. S. McCarthy
Institute of Nuclear and Particle Physics, Department of Physics, University of Virginia, Charlottesville, Virginia 22901
(Received 26 August 1993)

Deep inelastic polarized and unpolarized structure functions for a free nucleon are obtained in a modified center-of-mass bag model, which includes the symmetry-breaking effects from spin-dependent interactions. The quark distribution functions, calculated at $Q_0^2 \simeq (0.9\ \mathrm{GeV}/c)^2$, are evolved to a higher Q^2 region and compared with the data and other models. The model gives a reasonable description for the valence part of the structure functions at $x > 0.3$. For the small-x region, the contributions from the sea are necessary. The spin-dependent effects are important in describing the existing data.

PACS number(s): 13.60.Hb, 12.39.Ba

I. INTRODUCTION

It is well known that quantum chromodynamics (QCD), the theory of interactions of quarks and gluons, provides a basic description of strong interactions in the standard model. For high-energy scattering processes, the cross section can be factorized into a *hard* piece, the parton cross section which can be calculated in the framework of perturbative QCD, and a *soft* piece which depends on the parton distribution functions inside the nucleon. In the QCD quark parton model, at the leading order, the structure functions in the deep inelastic lepton-nucleon scattering are "charge" squared weighted combinations of the quark distribution functions $q_{f,h}(x)$, which denotes the probability of finding a quark with flavor f, momentum fraction x, and helicity h within the nucleon. These distribution functions are essentially determined by the quark-gluon structure of the nucleon. Since these functions play an important role in standard model phenomenology and in understanding the nucleon structure, many recent experiments have been done to measure deep inelastic unpolarized structure functions and extract the parton distribution functions. (See [1,2] for the review of deep inelastic structure functions, [3] for a comprehensive compilation of the latest deep inelastic data and [4,5] for the comparisons of data from different measurements.)

Among the unpolarized data, recent deep inelastic scattering data provide some new information of the internal structure of the nucleon. In particular, from the recent New Muon Collaboration (NMC) measurement [6] of difference $F_2^p - F_2^n$ the Gottfried sum rule [7] is found to be significantly less than the quark-parton model prediction of 1/3. This implies that the down sea is larger than the up sea. Combining with a smaller strange sea from neutrino scattering [8,9], it seems likely that the unpolarized sea is not only SU(3) flavor asymmetric, but also SU(2) flavor asymmetric (i.e., the down sea and up sea are not equal). However, an SU(2) flavor symmetric sea is usually assumed.

*Electronic address: XS3E@VIRGINIA.EDU

For the polarized structure functions, many experiments [10–12] have been performed in the past two decades. A review of earlier works can be found in [13]. The recent measurement from the European Muon Collaboration (EMC) at CERN shows [12] that the first moment of g_1^p is significantly below the value expected from the Ellis-Jaffe sum rule [14]. Furthermore, the EMC data combined with the Bjorken sum rule [15] and the hyperon β-decay data indicate that only a small fraction of the proton's spin is carried by the spin angular momentum of the quarks, which seems to contradict the naive expectations from the low energy constituent quark models. These conclusions are confirmed by two most recent experimental results reported by the Spin Muon Collaboration (SMC) [16] and E142 [17] within large errors. At first glance the E142 data seem to disagree with the Bjorken sum rule, but a detailed analysis given by Ellis and Karliner [18] shows that the discrepancy between the conclusions drawn by the SMC and E142 data can be eliminated if the Q^2 variation and higher twist effects are taken into account.

There are a variety of theoretical activities attempting to resolve the quantitative decomposition and the origin of the spin of the nucleon. For an incomplete list of recent works and review on this topic see [19–22] and [23–26], and references therein. In principle, one should be able to calculate the parton distribution functions from the basic equations of QCD which determine the quark-gluon structure of the nucleon. We need to know the basic constituents inside the nucleon and QCD (perturbative and nonperturbative) interactions among these constituents; hence, the structure of the nucleon in QCD is remarkably complex. The lattice QCD [27] has provided a framework of evaluating the hadron structure (masses, quark-antiquark potential, and other low energy observables) in the nonperturbative way. Several preliminary results [28,29] of the quark-spin fraction of the nucleon spin have been reported. In [29], the quark loop (or "sea" quark) contributions are calculated. Even so, the evaluation of the structure functions and parton distribution functions is still not accessible in lattice approach and has to resort to various QCD-inspired nucleon models.

The first pioneering work of using the MIT bag model to calculate deep inelastic (unpolarized) structure func-

tions was made by Jaffe [30]; then the polarized structure functions were calculated in the same model by many authors (Hughes [31], Bell [32], and Celenza and Shakin [33]) and recently by Jaffe and Ji [34]. Since the momentum is not conserved in the intermediate state in the MIT bag model the structure function does not vanish for $x \geq 1$. An attempt to remove this difficulty by restoring the four-momentum conservation and including the effects of spectator quarks was given in the c.m. (center-of-mass) bag model [35]. The main idea of the model is that instead of the single quark current in the MIT bag model a covariant effective electromagnetic current of the nucleon was suggested. The current includes not only the piece of the struck quark but also the pieces of the spectator quarks. The current satisfies translational invariance so four momentum is conserved. Another approach to avoid the support problem in the MIT bag model was suggested by Benesh and Miller [36]. The Peierls-Yoccoz projection [37] has been used to obtain an eigenstate of zero momentum. Including pion corrections the valence structure functions of the nucleon and Δ are calculated. Another disadvantage of the original MIT bag model is that the spin-dependent force effect, which has been used to explain successfully the hadron spectroscopy [38], was neglected, hence, $F_2^n(x)/F_2^p(x)=2/3$ is a constant in disagreement with data. Many models [39–43] have been suggested to incorporate the spin-dependent effects in describing the inelastic structure functions. In Ref. [39], the nucleon is considered as a composite system of a quark and a pointlike diquark. The model treats kinematics relativistically and considers the spin-flavor dependence in the nucleon wave function. In Ref. [40], the effect of one-gluon exchange, yielding the $N - \Delta$ mass difference, is incorporated and significantly modifies the result given in the SU(6)-symmetric model. In [41], the structure functions are calculated by using two phenomenological nucleon models – the nontopological soliton (NTS) model and color-dielectric (CD) model. For the NTS model, the authors conclude that an agreement between xg_1^p and the EMC data could be obtained even if the proton wave function is SU(6) symmetric. As the authors of [39] pointed out, however, the model they considered cannot reproduce the large body of low energy data. In Ref. [42], the nucleon, which consists of three confining quarks, is treated approximately as an infinite free Fermi gas system at finite temperature. In [43], the constituent quark model [44] of the nucleon is used. In both [42] and [43], only unpolarized structure functions are calculated. Most of these model results are fairly close and can compare with the data in spite of different assumptions used in different models. It should be noted that a common feature of all these calculations is that the structure functions are evaluated at some very low momentum transfer scale ${Q_0}^2$ (e.g $\sim$ 0.063 GeV^2 for Ref. [39] and [43], $\sim$ 0.068 GeV^2 for Ref. [40], $\sim$ 0.09 GeV^2 for Ref. [41], and $\sim$ 0.06 GeV^2 for Ref. [42]); then these functions are evolved to the higher Q^2 region by using leading-order perturbative QCD. The problem, as pointed out by the authors of Ref. [39], is that "in order to obtain the correct momentum sum rule, it is necessary to go to extreme value of strong coupling constant $\alpha_s \geq 3 - 4$. Therefore the use of QCD perturbation theory at the leading order cannot be justified." We will show, however, that one may avoid this ambiguity and still obtain a reasonable description of deep inelastic structure functions from the low-energy nucleon model.

Recently, we suggested a modified (m.c.m.) bag model [45], based on the c.m. bag model in [35], to calculate both elastic form factors and deep inelastic structure functions. In [45], the symmetry-breaking effects coming from perturbative one-gluon exchange mechanism (color hyperfine interactions) and/or nonperturbative instanton spin interactions are simulated by introducing a symmetry-breaking parameter. It has been shown that by including spin force effects, the model gives a fairly good description for the magnetic moments of octet baryon and the electromagnetic form factors of the nucleon. We also show briefly in [45] that the same model can fairly describe many aspects of deep inelastic structure functions of the nucleon. In this paper, we present detailed results of these calculations.

The paper is organized as follows. In Sec. II, we will define the notation and give the basic formalism of the model calculation of the structure functions, and list the approximations used in the model. In Sec. III, the unpolarized structure functions F_1 and F_2 are derived from the hadronic tensor. In the Bjorken limit, these functions are scaling and satisfy the Callen-Gross relation. The valence quark distribution functions $xu_v(x, Q_0^2)$, $xd_v(x, Q_0^2)$ are evaluated around $Q_0^2 \simeq (0.9\ \mathrm{GeV}/c)^2$ from the model and then evolved to $Q^2 = 4$, 10.7, and 15 $(\mathrm{GeV}/c)^2$ by using leading order perturbative QCD evolution equations [46] and the analytical approach developed in [47]. Including the sea contributions, the structure functions F_2^p, F_2^n, $F_2^p - F_2^n$, the integral $\int_0^1 dx[F_2^p - F_2^n]_{\mathrm{val}}/x$ and the ratio F_2^n/F_2^p are compared with data and those from other models. In Sec. IV, the spin-dependent structure functions g_1 and g_2 are derived in the model. The polarized quark distributions, $\Delta u_v(x, Q^2)$, $\Delta d_v(x, Q^2)$, and their first moments are evaluated in the model at the same Q_0^2 and then evolved to higher Q^2 region [48]. The polarized sea quark distributions are discussed. Using the Bjorken sum rule, EMC data, ν-p scattering data and the model results of Δu_v and Δd_v, a set of sea quark polarizations is obtained. Including the sea contribution, the $xg_1^{(p)}(x)$, $xg_1^{(n)}(x)$, and $g_1^d(x)$ are compared with the latest data [12,16,17]. In Sec. V, the second spin-dependent structure function $g_2(x)$, the Burkhardt-Cottingham sum rule [49] and the higher twist effects are briefly discussed. A summary is drawn in Sec. VI. Derivations of some formulas are given in Appendixes A and B.

II. KINEMATICS AND HADRONIC TENSOR

In the one photon exchange approximation, the deep inelastic structure functions can be extracted from the hadronic tensor, which is the Fourier transformation of the single nucleon matrix element for the commutator of two electromagnetic currents:

$$W_{\mu\nu}(P,q,S) = \frac{1}{4\pi}\int d^4y e^{iqy}\langle P,S \mid [J_\mu(y), J_\nu(0)] \mid P,S\rangle \tag{2.1}$$

where $J_\mu(y)$ is the hadronic electromagnetic current which depends on the nucleon model one used, P^μ and S^μ are the four-momentum and spin vector of the target nucleon ($P^\mu P_\mu = M^2$, M is nucleon mass; $S^\mu S_\mu = -1$ and $P^\mu S_\mu = 0$), respectively. The initial nucleon state is covariantly normalized: $\langle P,S \mid P',S'\rangle = (2\pi)^3 2P^0\delta^3(\mathbf{P}-\mathbf{P}')\delta_{SS'}$ and q^μ is the four-momentum of the virtual photon. The conventional kinematical variables Q^2 and ν (or Q^2 and x) are defined as $Q^2 \equiv -q^2 > 0$ and $x \equiv Q^2/2M\nu$ ($\nu = P\cdot q/M$) with $0 \le x \le 1$.

$W_{\mu\nu}$ in (2.1) can be decomposed into two parts:

$$W_{\mu\nu} = W^{(S)}_{\mu\nu} + iW^{(A)}_{\mu\nu}, \tag{2.2}$$

where

$$W^{(S)}_{\mu\nu} = (-g_{\mu\nu} + q_\mu q_\nu/q^2)W_1(x,Q^2) + (P_\mu - q_\mu P\cdot q/q^2)(P_\nu - q_\nu P\cdot q/q^2)W_2(x,Q^2)/M^2 \tag{2.3}$$

and

$$W^{(A)}_{\mu\nu} = \epsilon_{\mu\nu\lambda\sigma}q^\lambda\{S^\sigma MG_1(x,Q^2) + [(P\cdot q)S^\sigma - (q\cdot S)P^\sigma]G_2(x,Q^2)/M\} \tag{2.4}$$

represent, respectively, the symmetric and antisymmetric parts of the tensor, from which the structure functions F_1, F_2 and G_1, G_2 are defined. In the deep inelastic region, these structure functions become the scaling functions of the Bjorken variable x only, i.e., in the Bjorken limit ($Q^2 \to +\infty$, $\nu \to +\infty$ with x fixed)

$$MW_1(x,Q^2) \to F_1(x)\ , \quad \nu W_2(x,Q^2) \to F_2(x) \tag{2.5}$$

and

$$M^2\nu G_1(x,Q^2) \to g_1(x)\ , \quad M\nu^2 G_2(x,Q^2) \to g_2(x). \tag{2.6}$$

The main purpose of this paper is to calculate these structure functions by using the current J_μ given in the modified c.m. bag model. The assumptions or approximations we used are listed below.

(a) The effective nucleon current is the sum of a single quark current, i.e., the virtual photon interacts with only one quark (struck quark) at a time and the other two quarks are spectators; this is the impulse approximation.

(b) The nucleon is assumed to be in the Fock state which only consists of three valence quarks. 56-plet SU(6) wave functions for the proton and neutron with spin up are used; the symmetry-breaking effect is described in terms of a parameter [45] $\xi \equiv R^p_d/R^p_u < 1$, which simulates the smaller spatial size for the scalar $u-d$ quark pair than that for the vector $u-u$ or $d-d$ quark pairs in the nucleon.

(c) The effect of quark confinement is described in terms of a bound state quark spatial wave function, which is basically determined by the large-scale structure of the nucleon.

Based on approximations (**a**) and (**b**), the γNN vertex can be written [45]

$$\int d^4y e^{iq\cdot y}\langle p' \mid J_\mu(y) \mid p\rangle = (2\pi)^4\delta^4(p+q-p') < p' \mid J_\mu(0) \mid p >$$
$$= (2\pi)\delta^4(p+q-p')\sum_{1\to 2,3}\int\left(\prod_{i=1}^3 d^3\mathbf{r}_i\right)e^{i\mathbf{q}\cdot\mathbf{r}_1}, \bar{q}_{p',\alpha'}(\mathbf{r}_1,\mathbf{r}_2,\mathbf{r}_3)[\hat{e}_q\gamma_\mu]_1 q_{p,\alpha}(\mathbf{r}_1,\mathbf{r}_2,\mathbf{r}_3) \tag{2.7}$$

where the δ function comes from the center-of-mass motion. The integral on the right-hand side (RHS) of (2.7) denotes the contribution coming from the γqq interaction and quark internal motion, where subscript 1 of the operator $[\hat{e}_q\gamma_\mu]_1$ denotes that the virtual photon interacts with the first (struck) quark and subscripts 2 and 3 denote the spectators. The summation runs over three quarks ($1 \to 3$). The nucleon wave function in (2.7) is

$$q_{p,\alpha}(\mathbf{r}_1,\mathbf{r}_2,\mathbf{r}_3) = \prod_{i=1}^3 q_{p,m}(\mathbf{r}_i)\alpha_N \tag{2.8}$$

where α_N is the SU(6) spin-flavor wave function of the nucleon, and the antisymmetric color wave function has been omitted. In (2.8), $q_{p,m}(\mathbf{r}_i)$ are the spin$-1/2$ bound quark wave functions. To calculate the Lorentz tensor $W_{\mu\nu}$, we use the nucleon rest frame. In this frame only the rest frame wave functions $q_m(\mathbf{r}_i)$ are involved, they can be described by, for instance, the cavity solution in the MIT bag model [30] or other bound quark wave function in the relativistic quark model [see (9), (10), (19) and (20) in Appendix A].

Using the current (2.7), the hadronic tensor (2.1) can be written as

$$W_{\mu\nu}(P,q,S)=\sum_{1\to 2,3}\sum_{\alpha_1,m_1} b_{\alpha_1,m_1}(1;23)\frac{M}{(2\pi)^6 R_1^3}\int\prod_{i=1}^{3}\frac{d^3\mathbf{k}_i}{2k_i}\delta^4(q+P-\sum_i k_i)I_{m_1\mu\nu}(\mathbf{k}_1-\mathbf{q})I_{m_2}(\mathbf{k}_2)I_{m_3}(\mathbf{k}_3) \quad (2.9)$$

where $b_{\alpha_1,m_1}(1;23)=\langle\alpha_N \mid [b^\dagger_\alpha(m)\hat{e}_q^2 b_\alpha(m)]_1 \mid \alpha_N\rangle$ is the matrix element of $\hat{e}_q^2$ (the charge square operator of the struck quark), $\mathbf{k}_i$ and m_i are the three-momentum and spin projection of ith quark, and R_i $(i=1,2,3)$ are the parameters appearing in the wave functions of the struck quark $(i=1)$ and spectator quarks $(i=2,3)$ which determine the radius of the quark distributions (see Appendix A). The integral

$$I_{m_1,\mu\nu}(\mathbf{k}_1-\mathbf{q})\equiv\int d^3\mathbf{r}_1\int d^3\mathbf{r}_{1'}e^{i(\mathbf{k}_1-\mathbf{q})\cdot(\mathbf{r}_1-\mathbf{r}_{1'})}\bar{q}_{m_1}(\mathbf{r}_1)\times\gamma_\mu \not{k}_1\gamma_\nu q_{m_1}(\mathbf{r}_{1'}) \quad (2.10)$$

denotes the contribution coming from the struck quark which interacts with the virtual photon which carries four-momentum $q=(q_0,\mathbf{q})$ while

$$I_{m_j}(\mathbf{k}_j)\equiv\int d^3\mathbf{r}_j\int d^3\mathbf{r}'_j e^{i\mathbf{k}_j\cdot(\mathbf{r}_j-\mathbf{r}_j')}\bar{q}_{m_j}(\mathbf{r}_j)\times\gamma_0\not{k}_j\gamma_0 q_{m_j}(\mathbf{r}'_j)\qquad (j=2,3) \quad (2.11)$$

denotes the contributions from the spectator quarks. The δ function in (2.9) guarantees four-momentum conservation.

Using the identity $\gamma_\mu\gamma_\lambda\gamma_\nu = S_{\mu\lambda\nu\sigma}\gamma^\sigma + i\epsilon_{\mu\nu\lambda\sigma}\gamma^\sigma\gamma^5$, where $S_{\mu\lambda\nu\sigma}=g_{\mu\lambda}g_{\nu\sigma}+g_{\mu\sigma}g_{\nu\lambda}-g_{\mu\nu}g_{\lambda\sigma}$, the integral (2.10) can be rewritten as

$$I_{m_1,\mu\nu}(\mathbf{k}_1-\mathbf{q})=S_{\mu\lambda\nu\sigma}k_1{}^\lambda I^{(s)\sigma}(\mathbf{k}_1-\mathbf{q})-i\epsilon_{\mu\nu\lambda\sigma}k_1{}^\lambda I^{(A)\sigma}_{m_1}(\mathbf{k}_1-\mathbf{q}) \quad (2.12)$$

in which the symmetric term $I^{(s)\sigma}(\mathbf{k}_1-\mathbf{q})$ is independent of the quark spin projection and contributes to the unpolarized structure functions $F_1(x)$ and $F_2(x)$, while the antisymmetric term $I^{(A)\sigma}_{m_1}(\mathbf{k}_1-\mathbf{q})$ depends on the quark spin projection and generates the polarized structure functions $g_1(x)$ and $g_2(x)$. We will discuss them separately.

III. UNPOLARIZED STRUCTURE FUNCTIONS

A. Formalism

Using standard projection operators and (2.9), we obtain W_1 and W_2 as (see Appendix A)

$$W_i=\sum_{1\to 2,3}\sum_{\alpha_1,m_1} b_{\alpha_1,m_1}(1;23)\frac{M}{(2\pi)^6 R_1^3}\int\prod_{j=1}^{3}\frac{d^3\mathbf{k}_j}{2k_j}\delta^4(q+P-\sum_j k_j)I^{(i)}_{m_1}(\mathbf{k}_1-\mathbf{q})I_{m_2}(\mathbf{k}_2)I_{m_3}(\mathbf{k}_3)\qquad (i=1,2) \quad (3.1)$$

where $I_{m_j}(\mathbf{k}_j)$ $(j=2,3)$ are the spectator contributions in the momentum space and have been defined in (2.11). $I^{(i)}_{m_1}(\mathbf{k}_1-\mathbf{q})$ is the struck quark contribution and is projected out from (2.10) by using (2.12). Their expressions are given in Appendix A. It turns out that $I^{(i)}_{m_1}(\mathbf{k}_1-\mathbf{q})$, $I_{m_2}(\mathbf{k}_2)$ and $I_{m_3}(\mathbf{k}_3)$ are independent of the quark spin projections m_i. Hence the subscript m_1 in $\sum_{\alpha_1,m_1} b_{\alpha_1,m_1}(1;23)$ can be omitted. Using the bag-type quark wave function (See (10) in Appendix A) and completing the integrals over $\prod_{j=1}^{3} d^3\mathbf{k}_j$, we obtain

$$W_1(x,Q^2)=N(1+\eta/2)\sum_{1\to 2,3}C(1;23)\sum_\alpha b_\alpha(1;23)I_\alpha(R_1;\xi_2,\xi_3), \quad (3.2)$$

$$W_2(x,Q^2)=[\eta(1+3\eta/2)/(1+\eta/2)]W_1(x,Q^2), \quad (3.3)$$

where N is a normalization constant, $\eta\equiv 1/(1+\nu^2/Q^2)$, $\xi_i\equiv R_i/R_1$ $(i=2,3)$, $C(1;23)\equiv MR_1\xi_2^3\xi_3^3$ and $I_\alpha(R_1;\xi_2,\xi_3)$ is a dimensionless integral which presents the collective contribution from three valence quarks. The detail expression of $I_\alpha(R_1;\xi_2,\xi_3)$ is given in (17) and (18) in Appendix A.

If we neglect the symmetry-breaking effects coming from spin-dependent interactions, then $R_2=R_3=R_1=R$, $\xi_2=\xi_3=\xi_1=1$, and I_α does not depend on α, i.e., quark flavor, then (3.2) and (3.3) reduce into the SU(6) symmetric result [35]. We note that in the SU(6) symmetric limit, one has $\sum_\alpha b_\alpha=1$ for the proton and $\sum_\alpha b_\alpha=2/3$ for the neutron; it then leads to $F_2^n(x)/F_2^p(x)=2/3$ [30].

It is easy to verify, from (3.2)and (3.3), that in the Bjorken limit, $\eta\to 2Mx/\nu\to 0$ and $W_2/W_1=\eta(1+3\eta/2)/(1+\eta/2)\to 2Mx/\nu$. Hence one obtains

$$\nu W_2\to 2xMW_1,\qquad \text{i.e.,}\quad F_2(x)=2xF_1(x);$$

this implies that in the Bjorken limit the Callen-Gross relation is satisfied within the model. Furthermore, in Appendix A we briefly demonstrate the scaling behavior of the structure functions; i.e., both $F_1(x)$ and $F_2(x)$ are

scaling in the Bjorken limit and vanish when $x \to 1$. Numerical calculations also confirm this conclusion.

Since b_α in (3.2) is the matrix element of $\hat{e}_q^2$, it is easy to rewrite (3.2) into

$$F_1(x) = \frac{1}{2}\sum_q e_q^2 f_q(x), \tag{3.4}$$

where the quark distribution function $f_q(x)$ is determined by the model result $I_\alpha(R_1;\xi_2,\xi_3)$. Similarly we have

$$F_2(x) = x\sum_q e_q^2 f_q(x); \tag{3.5}$$

these are the parton model formulas as expected, because the impulse approximation (**a**) used in our model is the same approximation used in the parton model. In fact, the parton model formulas (3.4) and (3.5) can also be obtained in any nucleon model as far as the impulse approximation is imposed. However, the magnitude and shape of the quark distributions depend on approximations (**b**) and (**c**). We note that in our model only the three-valence quark configuration is considered; hence, the model result of the quark distributions should be identified with the valence part only.

B. Valence and sea decomposition

For later analysis, we divide the quark distribution functions $q(x)$ into two parts, one that comes from the three-valence quark configurations which the primitive quark model requires, the other from contributions of additional effects:

$$q_i(x) = q_{iv}(x) + q_{is}(x), \quad \bar{q}_i(x) = \bar{q}_{iv}(x) + \bar{q}_{is}(x), \tag{3.6}$$

where the subscripts v and s denote the terms "*valence*" and "*sea*." The *sea* contributions will be evaluated by using the QCD evolution approach with suitable inputs at some low Q^2 scale. By definition, we have $\bar{q}_{iv}(x) = 0$ ($\bar{q}_i = \bar{u}, \bar{d}, \bar{s}$), $s_v(x) = 0$ and $q_{is}(x) = \bar{q}_{is}(x)$. Then we have

$$F_2^p(x) = [F_2^p(x)]_{\rm val} + [F_2^p(x)]_{\rm sea}, \tag{3.7}$$

where

$$[F_2^p(x)]_{\rm val} = x[\frac{4}{9}u_v^p(x) + \frac{1}{9}d_v^p(x)] \tag{3.8}$$

and

$$[F_2^p(x)]_{\rm sea} = 2x[\frac{4}{9}u_s^p(x) + \frac{1}{9}d_s^p(x) + \frac{1}{9}s_s^p(x)], \tag{3.9}$$

small contributions coming from the charm quarks and other heavier quarks are neglected. The equality $q_s(x) = \bar{q}_s(x)$ satisfies the following condition: the sea is flavorless; i.e., the number of sea quarks with flavor f must be equal to the number of sea antiquarks with the same flavor. It should be noted that this condition only requires a weaker equality $\int_0^1 q_s(x)dx = \int_0^1 \bar{q}_s(x)dx$.

Using a symmetry breaking SU(6) wave function with a three-quark configuration, we obtain

$$u_v^p(x) = 4NMR\xi^3 I_u(R;1,\xi) \tag{3.10}$$

and

$$d_v^p(x) = 2NMR\xi^{-3} I_d(\xi R;\xi^{-1},\xi^{-1}), \tag{3.11}$$

where $R = R_u^p$. The integral $I_u(R;1,\xi)$ denotes $I_\alpha(R_u^p;\xi_2,\xi_3)$, in (3.2), with $\alpha = u$, $R_1 = R_u^p$, $\xi_2 = 1$ and $\xi_3 = R_d^p/R_u^p \equiv \xi$ ($\xi \le 1$). The same notation is used for $I_d(\xi R;\xi^{-1},\xi^{-1})$. Obviously, the I_u comes from the quark configuration $[u;u,d]$ or $[u;d,u]$ and I_d comes from the quark configuration $[d;u,u]$. In obtaining (3.10) and (3.11), the symmetry $I_{u,d}(1;2,3) = I_{u,d}(1;3,2)$ has been used, which can be verified from the explicit expression of $I_\alpha(R_1;\xi_2,\xi_3)$. In a similar manner, we can obtain the valence quark distributions $u_v^n(x)$ and $d_v^n(x)$ in the neutron and the result shows that

$$u_v^p(x) = d_v^n(x) \qquad \text{and} \qquad d_v^p(x) = u_v^n(x); \tag{3.12}$$

this is expected because the isospin symmetry for the nucleon wave function is assumed. Hence, we will omit the superscript p and n below and use $u_v(x)$ instead of $u_v^p(x)$ and so on. We note that in the SU(6) symmetry limit, $\xi = 1$, one obtains, from (3.10) and (3.11), $u_v(x) = 2d_v(x)$.

The calculation of the structure function or quark distributions in the deep inelastic region is divided into two steps: (i) The valence quark distribution functions at Q_0^2=(0.9 GeV/c)^2 are calculated *nonperturbatively* by using the nucleon model [under approximations (a)-(c)], (ii) using QCD evolution approach to evolve these (valence) quark distributions *perturbatively* to higher Q^2 region, e.g., Q^2 ~4, 10.7, and 15 (GeV/c)^2, where the experiments were performed.

C. Valence quark distributions

For the nonperturbative calculation in step (i), we need to determine the parameters in the model. One can see from (17) in Appendix A that there are only *three* parameters: R ($= R_u^p$), ξ ($= R_d^p/R_u^p$), and ϵ ($=|\ \mathbf{p}\ |_{\rm max}\ R$, where $|\ \mathbf{p}\ |_{\rm max}$ is the maximum value of three-momentum of the struck quark inside the nucleon). The former two have been determined from the fit of the rms radius of the neutron and proton [cf. Eq. (8) in [45]],

$$\langle r_n^2\rangle = -2[(1-\xi^2)/(4-\xi^2)][\langle r_p^2\rangle - 3/(2M^2)], \tag{3.13}$$

and the ratio [cf. Eqs. (9) and (10) in [45]],

$$\mu_n/\mu_p = -(2/3)\{1 - 8MR(1-\xi)/[4MR(8+\xi) + c]\} \tag{3.14}$$

where c is a constant. The results were R =5 (GeV/c)$^{-1}$ and ξ = 0.85, in this paper we take the same values in order to maintain the consistency. The third parameter ϵ is a new one and depends on the maximum momentum of the struck quark inside the nucleon. In the zero-temperature Fermi gas model, $|\ \mathbf{p}\ |_{\rm max}$ can be identified as the Fermi momentum; e.g., in Ref. [42], k_F = 0.2228 GeV/c is chosen for the u quark and k_F = 0.1539 GeV/c for the d quark. In our model, we choose $\epsilon = 3$ [for R =5 (GeV/c)$^{-1}$, it implies $|\ \mathbf{p}\ |_{\rm max}$=0.6 GeV/$c$] to constrain

TABLE I. Comparison of the calculated moments of unpolarized quark distribution functions and Gottfried sum rule given by different models with experiments.

Quantity	Data[a]	FG [42]	IK [43]	This paper
$\int_0^1 u_v(x)dx$	2.04±0.14	–	–	1.999[b]
$\int_0^1 d_v(x)dx$	1.07±0.20	–	–	0.986
$\int_0^1 xu_v(x)dx$	0.275±0.011	0.276	0.225	0.275
$\int_0^1 xd_v(x)dx$	0.116±0.017	0.114	0.109	0.123
$\int_0^1 xq_s(x)dx$	0.074±0.011	0.062	0.085	0.079
$[I_{\rm Gott}]_v$	0.333[c]	–	–	0.340
$[I_{\rm Gott}]_s$	–	–	–	−0.092
$I_{\rm Gott}$	0.240±0.016[d]	–	–	0.248

[a]Data are taken from [1] except $I_{\rm Gott}$.
[b]Input.
[c]Here $\int_0^1[u_v(x)-d_v(x)]dx=1$ has been used. Taking the data of $\int_0^1 u_v(x)dx$ and $\int_0^1 d_v(x)dx$ one obtains $[I_{\rm Gott}]_v$=0.323±0.081
[d]Ref. [6].

the valence quark distributions to satisfy the normalization conditions

$$\int_0^1 u_v(x)dx=2 \quad \text{and} \quad \int_0^1 d_v(x)dx=1, \quad (3.15)$$

which are satisfied within numerical error (see Table I).

For the perturbative calculation, the QCD scale parameter Λ is taken to be 0.3 GeV/c. The numerical results of $xu_v(x)$ and $xd_v(x)$ at Q^2=0.81 and 15 (GeV/c)^2 are shown in Figs. 1(a) and 1(b). For comparison, the results given in the Fermi gas model [42] and the constituent quark model [43] are shown. The main reason for choosing Q_0^2=0.81 (GeV/c)^2 as the renormalization scale is that the perturbative QCD can be used in a less ambiguous way above this scale. The running coupling constant $\alpha_s(Q^2)$ in the leading order in the modified minimal subtraction ($\overline{\rm MS}$) scheme (all quarks are assumed to be massless) is

$$\alpha_s(Q^2)=4\pi/[(11-2f/3)\ln(Q^2/\Lambda^2)]; \quad (3.16)$$

this leads to $\alpha_s \simeq 0.4-0.6$ for $f=3$ and the QCD scale parameter: $\Lambda=0.2-0.3$ GeV/c. We have tried two other different values of Q_0^2: (0.8 GeV/c)^2 and (1.0 GeV/c)^2; the result shows that the predictions for F_2^p and F_2^n etc. are not too sensitive to the Q_0^2 value provided that the normalization conditions (3.15) are imposed.

D. Results with sea contributions

For the sea quark distributions, we may assume, as many authors [39–43] do, that the sea and gluon distributions are zero at some very low Q_0^2, then use the leading-order QCD evolution approach to obtain the sea distributions in the higher Q^2 region. But it will face the ambiguity of using perturbative QCD. On the other hand, if we start from $Q_0^2 \simeq$1.0 (GeV/c)^2, then some initial input distributions for sea quarks and gluons at this scale are needed, but we do not have any information about these inputs at this scale. Hence we first evolve the valence quark distributions to Q^2 = 4 (GeV/c)^2, then combine with the usual parametrized inputs of gluon and sea quark distributions at this scale, and obtain the sea distribution in the higher Q^2 region. Hence our sea quark and gluon distributions are different from those in [42] and [43]. However, taking a very low Q_0^2 [<0.1 (GeV/c)^2] and assuming the initial sea and gluon distributions are

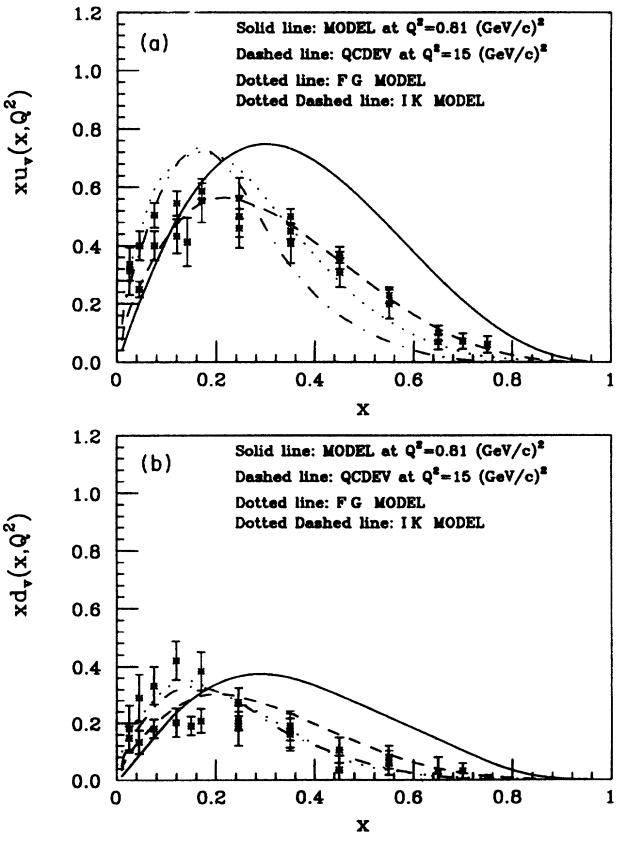

FIG. 1. (a) The calculated $xu_v(x,Q^2)$ at Q^2=0.81 (GeV/c)^2 (solid line) and QCD evolved result at Q^2=15 (GeV/c)^2 (dashed line) given in this paper. Data are taken from Ref. [1]. The results given by Fermi gas model [42] (dotted line) and constituent quark model [43] (dot-dashed line) are also shown. (b) Same as (a), but for $xd_v(x,Q^2)$.

approximately zero at this scale, we obtain, after evolution, almost the same results as those given by [42] and [43].

The unpolarized structure functions $[F_2^p(x)]_v$, $[F_2^p(x)]_{v+sea}$ and $[F_2^n(x)]_v$, $[F_2^n(x)]_{v+sea}$ are shown in Figs. 2(a) and 2(b). The unpolarized sea and gluon distributions given by this paper and other models are shown in Figs. 3(a) and 3(b), where $xq_s(x) = 2x[u_s(x) + d_s(x) + s_s(x)]$ is singlet quark distribution. To separate the different flavor contributions in the sea, we choose two options:

$$\text{(i)} \quad u_s(x) = d_s(x) \qquad \text{or} \qquad d_s(x) - u_s(x) = 0, \quad (3.17)$$

$$\text{(ii)} \quad u_s(x) < d_s(x) \qquad \text{or} \qquad d_s(x) - u_s(x) > 0; \quad (3.18)$$

both options require $s_s(x) = 0.25[u_s(x) + d_s(x)]$. Option (i) implies that sea violates SU(3) flavor symmetry but maintains SU(2) symmetry, while option (ii) means the sea even violates SU(2) flavor symmetry. The numerical results for the integrals $\int_0^1 xu_v dx$, $\int_0^1 xd_v dx$, and $\int_0^1 xq_s dx$ are listed in Table I. The comparisons of our F_2^p and F_2^n with other models are shown in Figs. 4(a) and 4(b), where an SU(2) flavor asymmetric sea, option (ii), has been used in our prediction. The result of $F_2^p(x) - F_2^n(x)$ and $[F_2^p(x) - F_2^n(x)]/x$ are shown in Figs. 5(a) and 5(b). A comparison of $F_2^p(x) - F_2^n(x)$ and $F_2^n(x)/F_2^p(x)$ given by different models are shown in Figs. 6(a) and 6(b) respectively.

E. Several remarks

From the results given above, we would like to make some remarks.

(i) One can see from Figs. 1(a) and 1(b) that qualitatively the results given by different models are the same. For xu_v, our result gives a better fit to the data than the Fermi gas model [42] and constituent quark model [43]. For xd_v, however, their results are better. As a consequence, our F_2^p agrees well with the data [Fig. 4(a)], but the F_2^n is somewhat higher than data in the region $x > 0.3$ [Fig. 4(b)]. For $0.1 < x < 0.3$, both F_2^p and F_2^n given by our model seem to be better than those from the other two models, this is because our sea contribution is closer to the data [Fig. 3(a)] in this x range. For very low x ($x < 0.1$), the model dependence is clearly seen; however, because of large theoretical uncertainties and

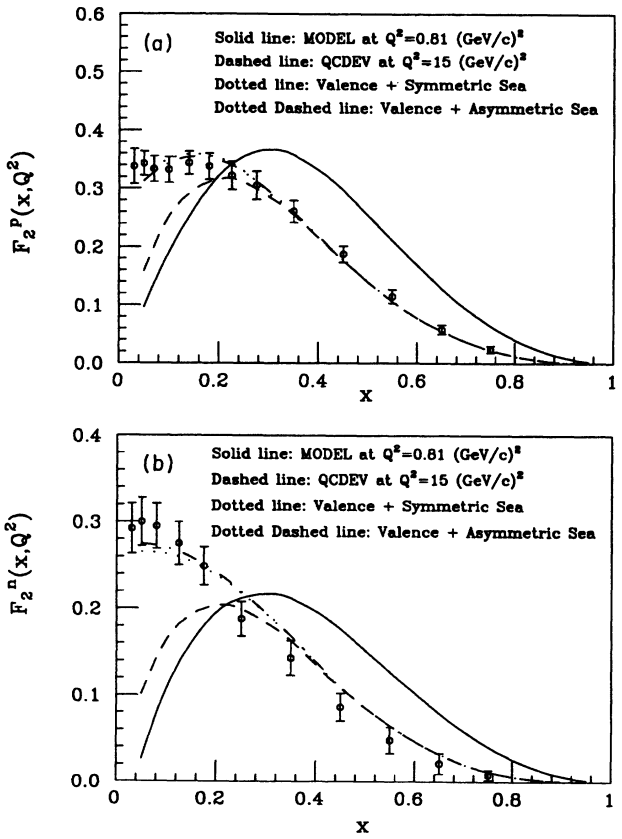

FIG. 2. (a) The calculated $[F_2^p(x, Q^2)]_{val}$ at Q^2=0.81 (GeV/c)^2 (solid line) and QCD evolved result at Q^2=15 (GeV/c)^2 (dashed line). $F_2^p(x, Q^2)$ (dotted line: valence + symmetric sea; dot-dashed line: valence + asymmetric sea) are compared with data [3]. (b) Same as (a), but for F_2^n.

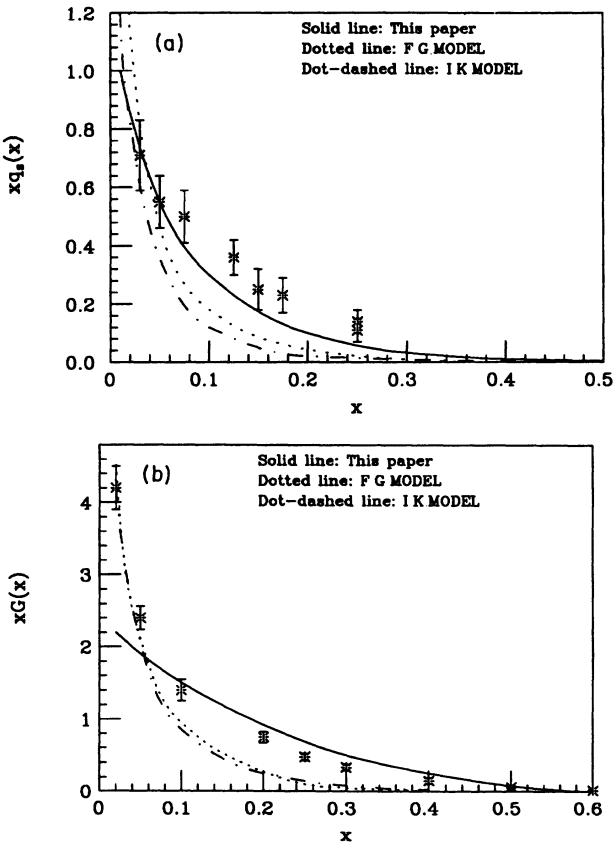

FIG. 3. (a) The calculated $xq_s(x)$ given in this paper (solid line) compared with data [1] at Q^2=15 (GeV/c)^2. The results given by Fermi gas model [42] (dotted line) and constituent quark model [43] (dot-dashed line) are also shown. (b) Same as (a), but for the unpolarized gluon distribution $xG(x)$.

data errors one cannot make a meaningful comparison between model results and data.

(ii) In the parton model, the integral $I_{Gott} \equiv \int_0^1 dx[F_2^p(x) - F_2^n(x)]/x$ would be 1/3 if the sea is SU(2) flavor symmetric. However, the NMC data show $I_{Gott}=0.240\pm0.016$. One can see from Fig. 5(b) that the model result of the valence quark contribution $[F_2^p(x) - F_2^n(x)]_{val}/x$ (dashed line) is higher than the data in the low-x region, while the sea contribution (dot-dashed line) given by (3.18), i.e., option (ii) leads to $[F_2^p(x) - F_2^n(x)]_{sea}/x < 0$, and the sum of valence and sea contributions is consistent with the NMC data [solid line in Fig. 5(b) or Fig. 5(a)]. The numerical results for the integrals are listed in Table I. Within our model, the difference between $F_2^{p,n}$ given by using a symmetric sea [option (i)] and asymmetric sea [option (ii)] is quite small and only appears in the small-x region ($x < 0.2$). However, this small difference could be the source which causes the violation of the Gottfried sum rule.

(iii) The NMC data seem to favor a flavor asymmetric sea. The idea that the sea might not be SU(2) symmetric was suggested by Feynman and Field [50] based on the Pauli exclusion principle. Since the proton contains two valence up-quarks but only one down-quark, the Pauli principle would suppress the creation of $u\bar{u}$ pairs relative to $d\bar{d}$ pairs. Ross and Sachrajda [51] showed that a nonzero value for $u_s(x) - d_s(x)$ can be obtained from higher-order QCD contributions. However, the effect given by perturbative QCD calculations is too small to explain the deviation of Gottfried sum rule (some earlier works [52,53] also found that the up-sea quark component is not identical with the down-sea component within the proton, the up-sea is larger than the down-sea). This means that a significant contribution should come from nonperturbative interactions. Many different explanations for the violation of Gottfried sum rule, have been suggested recently, an incomplete list includes Ref. [54–59]. We note that, however, the experimental data have large errors in the small-x region, where the sea is the dominate contribution; hence, more precise measurements of $F_2^p(x)$ and $F_2^n(x)$ at small-x region are needed in order to verify if, and to what extent, the Gottfried sum rule is violated.

(iv) The ratio $F_2^n(x)/F_2^p(x)$, as shown in Fig. 6(b), is sensitive to the spin dependent interactions. As discussed in [45] and [60] that the repulsion between $u - u$ pair comes from color magnetism which is based on perturbative QCD and derived from one-gluon exchange Breit-Fermi interactions, while the attraction between $u - d$ quark pair can only be induced by a nonperturbative mechanism, e.g., instanton interactions [61]. One can see from Fig. 6(b) that for $\xi = 0.85 < 1$ the model

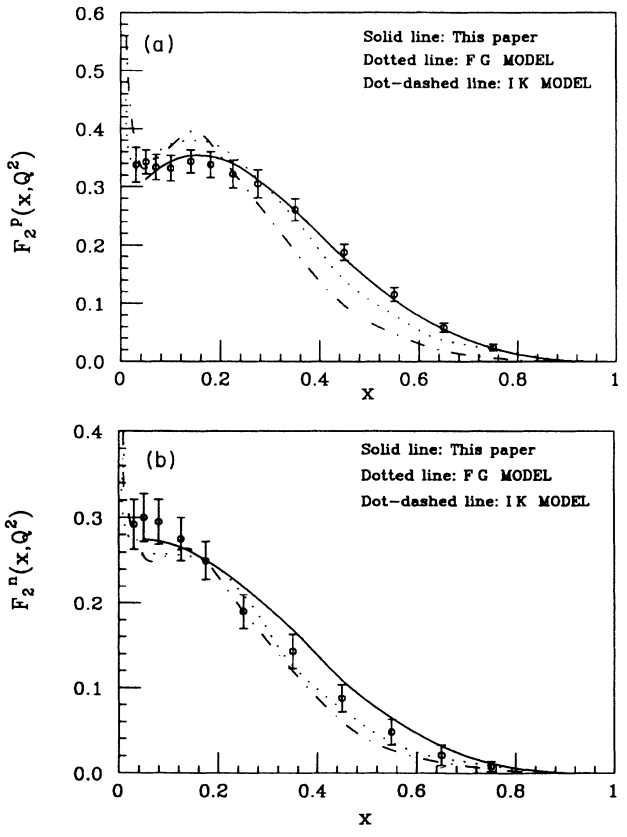

FIG. 4. (a) Comparison of our $F_2^p(x,Q^2)$ with other models. (b) Same as (a), but for $F_2^n(x,Q^2)$.

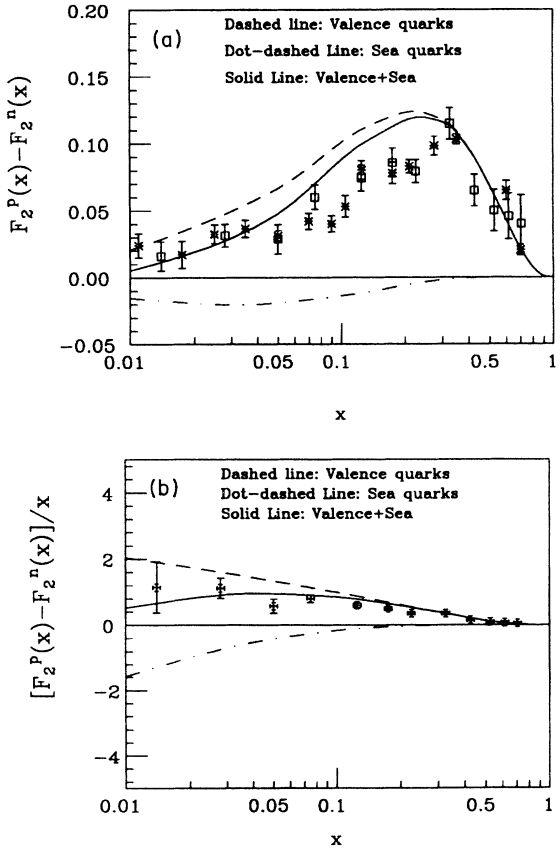

FIG. 5. (a) The calculated $[F_2^p(x) - F_2^n(x)]_{val}$ (dashed line), $[F_2^p(x) - F_2^n(x)]_{sea}$ (dot-dashed line), and $[F_2^p(x) - F_2^n(x)]_{val+sea}$ (solid line) data are taken from [6]. (b) Same as (a), but for $[F_2^p(x) - F_2^n(x)]/x$.

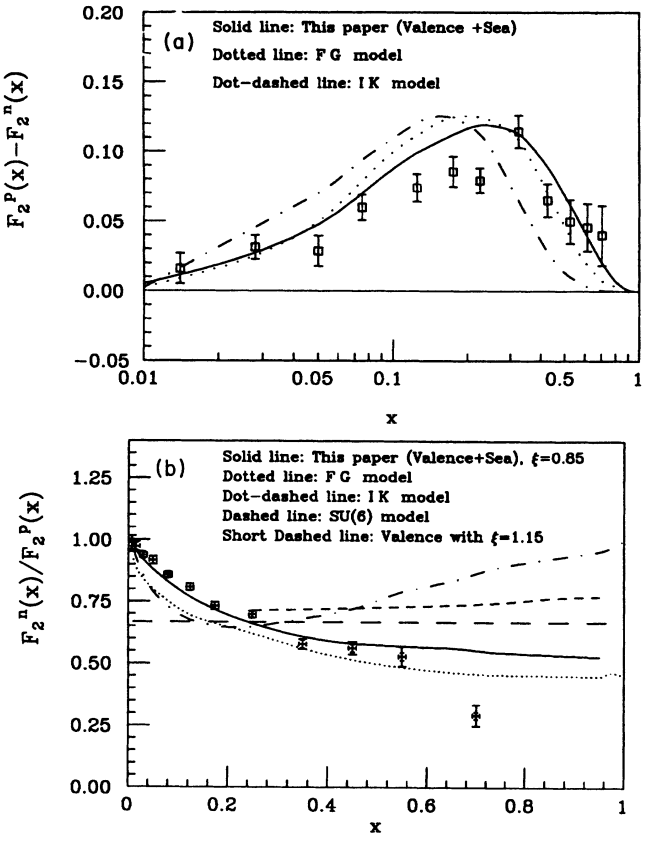

FIG. 6. (a) Comparison of our $F_2^p(x) - F_2^n(x)$ with other models (dotted line: [42] and dot-dashed line: [43]). (b). Comparison of $F_2^n(x)/F_2^p(x)$ with data and other models. Solid line (short-dashed line): this paper with ξ=0.85 (1.15), dotted line: [42], dot-dashed line: [43] and dashed line: SU(6) limit.

gives a reasonable x behavior of $F_2^n(x)/F_2^p(x)$ (except large-x region), while for $\xi = 1.15$ (which simulates a larger spatial size for the scalar $u-d$ quark pair than that for the vector quark pairs, that means the interaction between $u-d$ quark pair is more repulsive than that between $u-u$ or $d-d$ quark pairs) the prediction seems to conflict with the data. A similar result is also obtained in the light-cone constituent quark model (see [62]). It seems to imply that to obtain a correct large-x behavior of $F_2^n(x)/F_2^p(x)$, in addition to the one-gluon exchange effect, other mechanisms and nonperturbative contributions are needed.

IV. SPIN-DEPENDENT STRUCTURE FUNCTIONS

A. Formalism

The spin-dependent structure functions g_1 and g_2 can be extracted from the antisymmetric part of the hadronic tensor $W_{\mu\nu}^{(A)}$, Eq. (2.4). For convenience, we define two dimensionless quantities: $\pi^\mu \equiv P^\mu/M$ and $\rho^\mu \equiv q^\mu/\nu$, then we have $\pi^2 = 1$, $\rho^2 = -Q^2/\nu^2$, $S\cdot\pi = 0$, and $\rho\cdot\pi = 1$. Using these variables, (2.4) can be rewritten as

$$W_{\mu\nu}^{(A)} = \epsilon_{\mu\nu\lambda\sigma}\rho^\lambda\{S^\sigma g_1(x,Q^2) + [S^\sigma - (\rho\cdot S)\pi^\sigma]g_2(x,Q^2)\}. \tag{4.1}$$

On the other hand, the hadronic tensor can be calculated from the dynamical model of the nucleon in which the hadronic electromagnetic current and the nucleon state are known. From (2.9) and (2.12), we can write

$$W_{\mu\nu}^{(A)}(P,q,S) = \epsilon_{\mu\nu\lambda\sigma}\rho^\lambda I^\sigma(x,Q^2) \tag{4.2}$$

where $I^\sigma(x,Q^2)$ is obtained from (2.9) by changing $I_{m_1}(\mathbf{k}_1-\mathbf{q})$ into $I_{m_1}^{(A)\sigma}(\mathbf{k}_1-\mathbf{q})$ and

$$I_{m_1}^{(A)\sigma}(\mathbf{k}_1-\mathbf{q}) = (2\pi)^3\bar{\phi}_m(\mathbf{k}_1-\mathbf{q})\gamma^\sigma\gamma^5\phi_m(\mathbf{k}_1-\mathbf{q}). \tag{4.3}$$

Comparing (4.1) and (4.2), g_1 and g_2 can be easily obtained.

In the nucleon rest frame, $\pi^\mu = (1,0,0,0)$, $S^\mu = (0,0,0,1)$, and $\rho^\mu = (1,\mathbf{q}/\nu)$. Here the nucleon spin is chosen in the z direction and $|\mathbf{q}| = \nu(1+Q^2/\nu^2)^{1/2}$. For the direction of $\mathbf{q}$, we can choose (i) $\mathbf{q} \parallel -\mathbf{S}$ nucleon longitudinally polarized along $\mathbf{q}$ and (ii) $\mathbf{q}\perp\mathbf{S}$ nucleon transversely polarized along $\mathbf{q}$.

In the Bjorken limit, one has (i) $\rho\cdot S = 1$ for $\mathbf{q}\parallel -\mathbf{S}$, and (ii) $\rho\cdot S = 0$ for $\mathbf{q}\perp\mathbf{S}$. From these we have

$$g_1 = I_L^0 + I_L^3 \equiv g_L, \tag{4.4}$$

(i.e., light-cone "+" component of I_L) and

$$g_1 + g_2 = I_T^3 \equiv g_T, \tag{4.5}$$

where $I_L^{0,3}$ denote I^σ ($\sigma = 0,3$) in which the $\mathbf{q}$ is chosen in the opposite z direction and I_T^3 denotes I^3 in which the $\mathbf{q}$ is chosen in the opposite x direction. It is obvious that g_1 or g_L depends only on the "*longitudinal*" scattering and g_1+g_2 or g_T depends only on the "*transverse*" scattering, while g_2 is the difference between *transverse* scattering and *longitudinal* scattering. In the SU(6) symmetric limit, no special direction can be assigned for the nucleon system; hence, the rotational invariance requires that the *transverse* scattering and *longitudinal* scattering are equal and the difference between them, which is g_2, would be zero [63]. However, the symmetry-breaking effects lead to a nonvanishing g_2.

It can be shown from (2.9) and (2.12) that

$$W_{\mu\nu}^{(A)}(P,q,S) = \epsilon_{\mu\nu\lambda\sigma}\rho^\lambda\{2(N/\pi)C_0\nu\sum_{1\to2,3}\sum_{\alpha_1,m_1} b_{\alpha_1,m_1}(1;23)C(1;23)I_{\alpha_1,m_1}^\sigma(1;23)\} \tag{4.6}$$

where $I^{\sigma}_{\alpha,m}(1;23)$ (σ=0,3) are the dimensionless integrals and given in Appendix B. Since $I^{\sigma}_{\alpha,m}(1;23)$ depends on sgn(m), i.e., the sign of spin projection m of the struck quark, it naturally leads to the difference between spin-up and spin-down components, i.e., the spin-dependent structure functions. Comparing (4.6) with (4.2), one can obtain $I^{0,3}_{L}$ and I^{3}_{T}, then g_1 and g_2. Their expressions are listed in Appendix B.

Similar to the unpolarized case, from the term $\sum_{\alpha_1,m_1} b_{\alpha_1,m_1}(1;23)\mathrm{sgn}(m_1)$ in (4.6) [see (B3) and (B7) in Appendix B] one can rewrite $g_1(x)$ and $g_1(x)+g_2(x)$ into

$$g_1(x) = \frac{1}{2}\sum_q e_q^2[q_{\uparrow\parallel}(x) - q_{\downarrow\parallel}(x)], \tag{4.7}$$

$$g_1(x) + g_2(x) = \frac{1}{2}\sum_q e_q^2[q_{\uparrow\perp}(x) - q_{\downarrow\perp}(x)], \tag{4.8}$$

which determine the longitudinal and transverse spin structure functions. Similar to the unpolarized case, the scaling behaviour g_1 and g_2 can be obtained in the Bjorken limit, and they vanish when $x \to 1$.

B. Valence polarizations

The results of $\Delta u_v(x,Q^2)$ and $\Delta d_v(x,Q^2)$ at different Q^2 values are shown in Figs. 7(a) and 7(b). We emphasize that all parameters used here are the same as those in the unpolarized case: R=5 (GeV/c)^2, ξ = 0.85, and ϵ = 3, even the normalization factor N is unchanged. The valence components $[xg_1^p(x)]_{\rm val}$ and $[xg_1^n(x)]_{\rm val}$ are shown in Figs. 8(a) and 8(b). One can see from Fig. 8(a) that the valence contribution $[xg_1^p(x)]_{\rm val}$ at Q^2 = 10.7 (GeV/c)^2 (the dotted curve) is consistent with the data in the range of $x > 0.3$. This implies that the model gives a good description of the valence components of the spin-dependent structure functions, the difference between the $[xg_1^p(x)]_{\rm val}$ and data in the small-x region ($x < 0.3$) is naturally attributed to the polarized sea contributions. For comparison, the results given by Ref. [40] are shown in Fig. 8(a) and 8(b) (dashed curve). One can see that the results are very similar. For the $xg_1^p(x)$, both curves are very close and consistent with data at $x > 0.3$. Although their $xg_1^n(x)$ is larger than ours and becomes negative at $x < 0.02$, both curves are consistent with data within large errors.

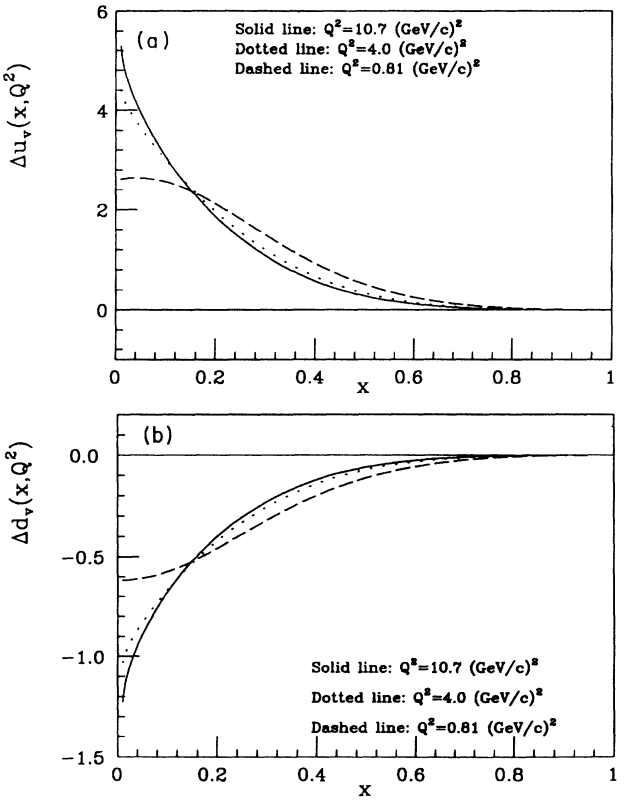

FIG. 7. (a) $\Delta u_v(x,Q^2)$ calculated from the model at Q^2=0.81, 4.0, and 15.0 (GeV/c)^2. (b) Same as (a), but for $\Delta d_v(x,Q^2)$.

C. Polarized sea and flavor decomposition of the proton spin

For the polarized sea quarks, no information about their distribution functions can be used as inputs at

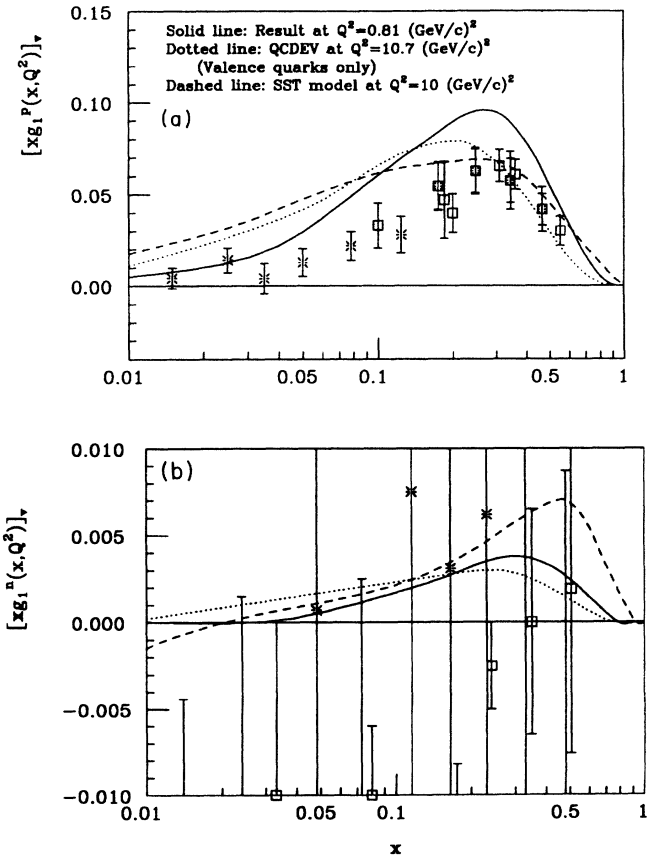

FIG. 8. (a) The calculated $[xg_1^p(x,Q^2)]_{\rm val}$ at Q^2=0.81 (GeV/c)^2 and QCD evolved result at Q^2=10.7 (GeV/c)^2, data is taken from [12]. The dashed curve is given by the SST model [40]. (b) Same as (a), but for $[xg_1^n(x,Q^2)]_{\rm val}$, data is taken from [16,17].

$Q_0^2 \simeq 1$ (GeV/c)^2 to evolve them to required higher Q^2 region. On the other hand, if we start from very low momentum transfer scale, e.g., $Q_0^2 \leq 0.1$ (GeV/c)^2 and assume that the sea and gluon polarizations are approximately zero at this scale, the leading-order QCD evolution would generate a positive polarized sea at higher Q^2 scale which seems to be inconsistent with the SMC result. Hence, we resort to a different analysis in this section.

Similar to the unpolarized case, from the quark-parton model we can write

$$g_1^p(x) = [g_1^p(x)]_{\rm val} + [g_1^p(x)]_{\rm sea}, \tag{4.9}$$

where

$$[g_1^p(x)]_{\rm val} = \frac{1}{2}[\frac{4}{9}c_u \Delta u_v(x) + \frac{1}{9}c_d \Delta d_v(x)] \tag{4.10}$$

and

$$[g_1^p(x)]_{\rm sea} = [\frac{4}{9}c_u \Delta u_s(x) + \frac{1}{9}c_d \Delta d_s(x) + \frac{1}{9}c_s \Delta s_s(x)], \tag{4.11}$$

where $\Delta u_v(x) = u_{v\uparrow}(x) - u_{v\downarrow}(x)$, $\Delta d_v(x) = d_{v\uparrow}(x) - d_{v\downarrow}(x)$, and $\Delta q_s(x) = \Delta \bar{q}_s(x)$ $(q = u, d, s)$ are assumed. In (4.10) and (4.11), the QCD radiative correction factors $c_u = 1 - (c_f - 1)\alpha_s/(2\pi)$ and $c_d = c_s = 1 - (2c_f - 1)\alpha_s/\pi$ are manifestly included, where $c_f = (33 - 8f)/(33 - 2f)$ with f, the number of quark flavors. Similar expressions for $[g_1^n(x)]_{\rm val}$ and $[g_1^n(x)]_{\rm sea}$ can be obtained by exchange $u \leftrightarrow d$.

From the model result we obtain

$$\Delta u_v \equiv \int_0^1 \Delta u_v(x)dx = 1.0003,$$
$$\Delta d_v \equiv \int_0^1 \Delta d_v(x)dx = -0.2217; \tag{4.12}$$

we note that these values will be slightly modified if different Q_0^2 are used. Hence, we would like to put 5% theoretical uncertainties on (4.12) and only present the uncertainties in the final result (see (4.18) below). (4.12) gives

$$\int_0^1 [g_1^p(x)]_{\rm val}dx = 0.1974, \int_0^1 [g_1^n(x)]_{\rm val}dx = 0.0106. \tag{4.13}$$

Hence,

$$\int_0^1 [g_1^p(x) - g_1^n(x)]_{\rm val}dx = 0.1868. \tag{4.14}$$

It implies that the valence parts almost saturate the Bjorken sum rule; i.e., the sea contributions to g_1^p and g_1^n are almost the same within the model. Using the Bjorken sum rule $\int_0^1 [g_1^p(x) - g_1^n(x)]dx = \frac{1}{6}(g_A/g_V)_{n\to p}[1 - \alpha_s/\pi - O(\alpha_s^2)]$=0.191 (where $\alpha_s \simeq 0.22$ has been used) and the EMC data

$$\int_0^1 g_1^p(x)dx = 0.126 \pm 0.018, \tag{4.15}$$

one obtains

$$\int_0^1 g_1^n(x)dx = -0.065 \pm 0.018. \tag{4.16}$$

Combining (4.13), (4.15), and (4.16) we have

$$\int_0^1 [g_1^p(x)]_{\rm sea}dx = -0.0714, \quad \int_0^1 [g_1^n(x)]_{\rm sea}dx = -0.0756. \tag{4.17}$$

Using the $\nu - p$ scattering data [64] $\Delta s \equiv \Delta s_s + \Delta \bar{s}_s = -0.15 \pm 0.09$, we obtain a set of sea polarizations:

$$2\Delta u_s = -0.229 \pm 0.021, \quad 2\Delta d_s = -0.257 \pm 0.033,$$
$$2\Delta s_s = -0.150 \pm 0.090. \tag{4.18}$$

From (4.18), we have $\Delta d_s \simeq 1.12\Delta u_s$, $\Delta s_s \simeq 0.31(\Delta u_s + \Delta d_s)$ (these asymmetric relations are very similar to those in the unpolarized case). Assuming the polarized sea quarks for different flavors have the same x behavior, which can be parametrized as

$$\Delta q_s(x) = a_q(2 - x)(1 - x)^{8.3} \quad (q = u, d, s), \tag{4.19}$$

where $a_u = -0.557$, $a_d = 1.122a_u$, and $a_s = 0.309(a_u + a_d)$. Using (4.19), the $[xg_1^p(x)]_{\rm sea}$ is calculated and the result is shown in Fig. 9(a) (dot-dashed curve), where the dotted curve is valence component only. The solid curve

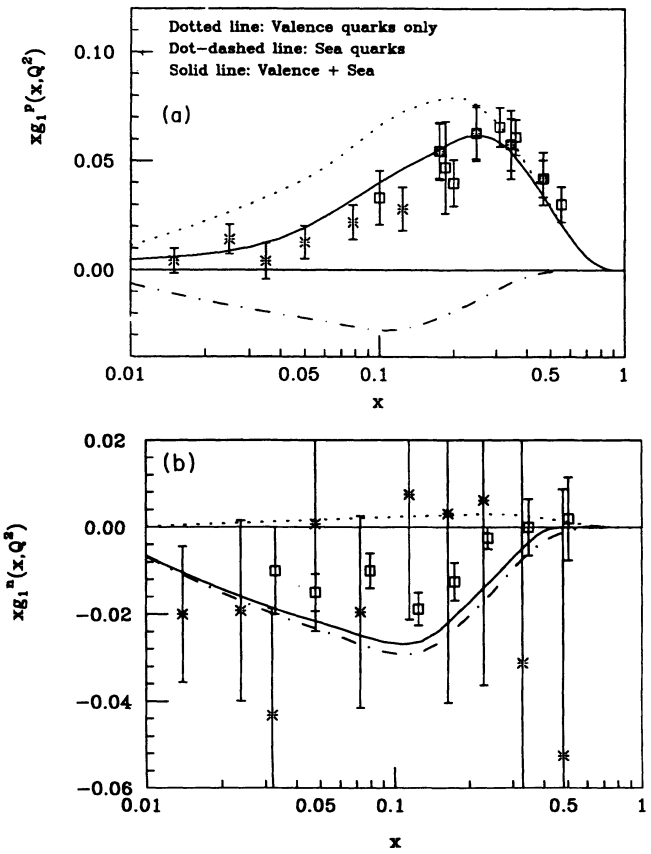

FIG. 9. (a) The calculated $[xg_1^p(x,Q^2)]_{\rm val}$ (dotted curve), $[xg_1^p(x,Q^2)]_{\rm sea}$ (dot-dashed curve), and $[xg_1^p(x,Q^2)]_{\rm val+sea}$ (solid curve, data is taken from Ref. [16]). (b) Same as (a), but for neutron, data is taken from [16,17].

shows the sum of valence and sea contributions. The corresponding curves for the $xg_1^n(x)$ are shown in Fig. 9(b). The result for $g_1^n(x)$ is shown in Fig. 10(a), data are taken from [16,17]. The result for $xg_1^d(x)$ is shown in Fig. 10(b). It shows that the theoretical predictions are consistent with data within large errors. The numerical results and comparison with other models are listed in Table II.

D. Several remarks

From the result given above, several observations are in order.

(i) In the static SU(6) limit, there are no sea contributions and

$$\Delta u_v = 4/3, \quad \Delta d_v = -1/3,$$
$$\Delta u_v = -4\Delta d_v, \quad \Delta u_v + \Delta d_v = 1; \tag{4.20}$$

i.e., 100% proton spin is contributed by the spin of the (valence) quarks. However, because of the presence of the quark-gluon interaction, which is described by quantum chromodynamics (QCD), quark-antiquark pairs and gluons (sea) are produced with the appropriate orbital angular momentum in addition to the usual three-valence quarks in the S state. It is obvious that the *valence* quarks can no longer be responsible for carrying 100% of the proton's spin. The result (4.12) shows

$$\Delta u_v \simeq 1.00, \quad \Delta d_v \simeq -0.22,$$
$$\Delta u_v \simeq -4.5\Delta d_v, \quad \Delta u_v + \Delta d_v \simeq 0.78. \tag{4.21}$$

It implies that even in the high Q^2 (deep inelastic) region the valence quarks' spin still contributes a large fraction of the proton spin. This result agrees with the earlier analysis by Close [65] [in [65] using $(g_A/g_V)_{n\to p} = 1.257 = \Delta u_v - \Delta d_v$ and assuming $\Delta u_v = -4\Delta d_v$, the author obtained $\Delta u_v \simeq 1.00$, $\Delta d_v \simeq -0.25$ and $\Delta u_v + \Delta d_v \simeq 0.75$].

(ii) The net sea quark spin polarization is -0.64, i.e., the spin of sea quarks is quite large and polarized against the proton spin. This means that although the valence quarks are still highly polarized, the sea quarks are spinning in the opposite direction and cancel most of the valence polarization [the cancellation occurs at small-x region, see Fig. 9(a)]. From (4.12) and (4.18), one obtains

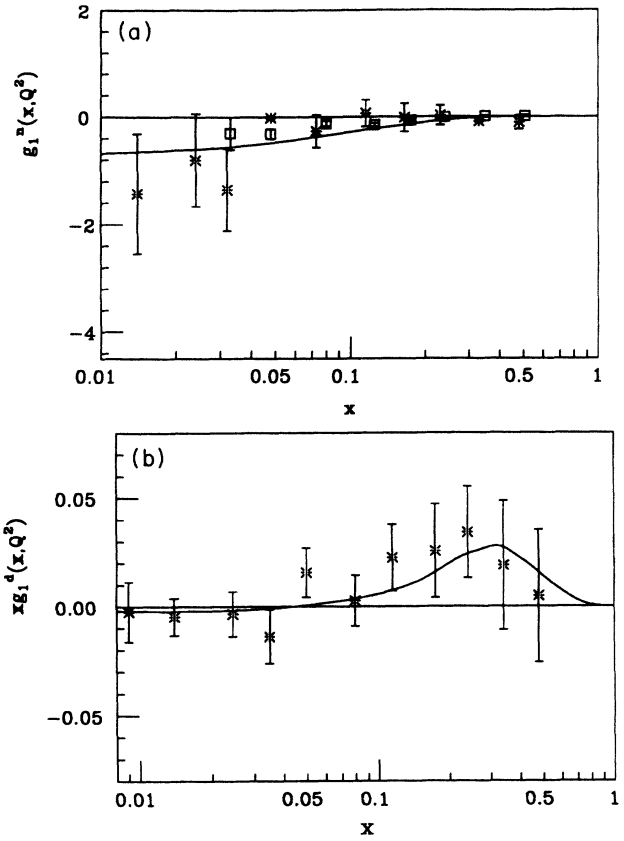

FIG. 10. (a) Same as Fig. 9(b), but for $g_1^n(x,Q^2)$. (b) Comparison of $[xg_1^d(x,Q^2)]$ with data [16,17].

TABLE II. Comparison of the calculated moments of polarized quark distribution functions and hyperon β-decay coupling constants given by different models with experiments.

Quantity	Data[a]	MIT [34]	SST [40]	This paper
Δu_v	–	0.840	0.951	1.0003
Δd_v	–	−0.210	−0.202	−0.2217
$\Delta u_s + \Delta\bar{u}_s$	–	0.0	–	−0.229
$\Delta d_s + \Delta\bar{d}_s$	–	0.0	–	−0.257
$\Delta s_s + \Delta\bar{s}_s$	−0.150±0.090[b]	0.0	–	−0.150[c]
F/D	0.58±0.02[d]	0.667	0.703	0.584
	0.575±0.016[e]			
$(g_A/g_V)_{n\to p}$	1.2573±0.0028	1.050	1.153	1.250
$(g_A/g_V)_{\Lambda\to p}$	0.718±0.015	0.630	0.701	0.723
$(g_A/g_V)_{\Sigma^-\to n}$	0.340±0.017	0.210	0.250	0.329
$(g_A/g_V)_{\Xi^-\to\Lambda}$	0.25±0.05	0.210	0.202	0.198

[a]Data are taken from [72] except $\Delta s_s + \Delta\bar{s}_s$ and F/D.
[b]Ref. [64].
[c]Input.
[d]Ref. [68].
[e]Ref. [73].

$$\Delta u = 0.771 \pm 0.054, \quad \Delta d = -0.479 \pm 0.035,$$
$$\Delta s = -0.150 \pm 0.090 \tag{4.22}$$

and

$$\Delta u + \Delta d + \Delta s = -0.142 \pm 0.110. \tag{4.23}$$

So that only 14% of the proton spin comes from the spin of quarks and antiquarks. The remaining 86% must come from other sources, e.g., the gluon polarization and the orbital angular momentum of the quarks and gluons.

(iii) The angular momentum sum rule [66] is

$$\frac{1}{2} = \frac{1}{2}\sum_q \Delta q + \Delta g + L_{q+g}, \tag{4.24}$$

where the first term on the RHS is the quark's spin contribution, Δg is the gluon spin polarization and L_{q+g} is the total orbital angular momentum of the quarks and gluons. Since $\sum_q \Delta q \simeq 0.14$, we have $\Delta g + L_{q+g} \simeq 0.43$. If we assume that $\Delta g \simeq L_{q+g} \simeq 0.22$, then the "*gluonic*" contribution [20,22] (due to the Adler-Bell-Jackiw axial anomaly) to the quark's spin polarization $\Delta\Gamma \equiv -[\alpha_s(Q^2)/2\pi]\Delta g(Q^2)$ would be very small ($\simeq -0.009$). Hence, our conclusion given above will not be affected by adding this gluonic term, except for the situation that $\Delta g(Q^2)$ is very large (e.g., see [23,67]). It should be noted that from leading order perturbative QCD evolution (e.g., see [48]), as Q^2 grows, the quark spin is conserved (Δq does not vary), and the gluon spin grows like $ln Q^2$, the total angular momentum conservation (4.24) requires L_{q+g} must grow in the negative direction to cancel Δg. However, $\Delta\Gamma$ does not vary due to $\alpha_s(Q^2) \sim 1/ln Q^2$.

(iv) It is easy to check that our result of flavor decomposition of the proton spin (4.22) can also accommodate the existing hyperon β−decay constants. Using $F + D = \Delta u - \Delta d$, $F - D = \Delta d - \Delta s$ and (4.22) we have $F = 0.461$, $D = 0.789$ and $F/D = 0.584$ (which agrees well with data from [68]). A comparison of the predicted hyperon β-decay constants with data and other models is shown in Table II. The quark polarizations (4.22) indeed gives a good fit to the existing data except for $(g_A/g_V)_{\Xi^-\to\Lambda}$.

(v) Combining our model result (4.13) with Bjorken sum rule and EMC data, the sea should be negatively polarized as shown in (4.18). However, as mentioned above a negatively polarized sea cannot be generated by leading-order perturbative QCD from very low Q_0^2 (if at this scale the sea and gluon polarizations are zero), and it must come from some nonperturbative mechanism. It is interesting to note that a preliminary lattice QCD result reported in [29] shows that the sign of quark loop ("sea") contribution to the isoscalar axial vector coupling constant g_A is *negative*. Another possible mechanism which may cause a negatively polarized sea is nonperturbative instanton interactions [69].

(vi) Similar to the unpolarized case, the polarized sea seems to be flavor asymmetric, see (4.18); at least it violates SU(3) flavor symmetry. In the unpolarized case, it is relatively easy to verify if the unpolarized sea violates SU(2) flavor symmetry by measuring the deviation of the Gottfried sum rule, because the u_v and d_v must obey the valence quark number sum rules in (3.15). In the polarized case no similar constraints exist. Hence the valence part of the $\int_0^1[g_1^p(x,Q^2) - g_1^n(x,Q^2)]dx$, i.e., $\frac{1}{6}\int_0^1[\Delta u_v(x,Q^2) - \Delta d_v(x,Q^2)]dx$ is unknown. To determine the sign of the sea term $\frac{1}{3}\int_0^1[\Delta u_s(x,Q^2) - \Delta d_s(x,Q^2)]dx$, one needs to measure $\Delta u_v(x,Q^2) - \Delta d_v(x,Q^2)$ independently in addition to g_1^p and g_1^n.

V. SECOND SPIN-DEPENDENT STRUCTURE FUNCTION

For the second spin-dependent structure function g_2, we will not discuss the sea contributions and only briefly present the results given by the valence contribution, so the subscript "val" will be omitted below. But bear in mind that these results, including only valence quarks, may have substantial modifications in the small-x region as we have seen in the g_1 case. The model results for $g_2^{(p,n)}$ are shown in Fig. 11(a). It can be shown that in the SU(6) symmetric limit (ξ=1), $g_1 = g_T$; hence, $g_2^{(p,n)}(x,Q^2) = 0$ and $\int_0^1 g_2^{(p,n)}(x,Q^2)dx = 0$; i.e., the Burkhardt-Cottingham (BC) sum rule is sat-

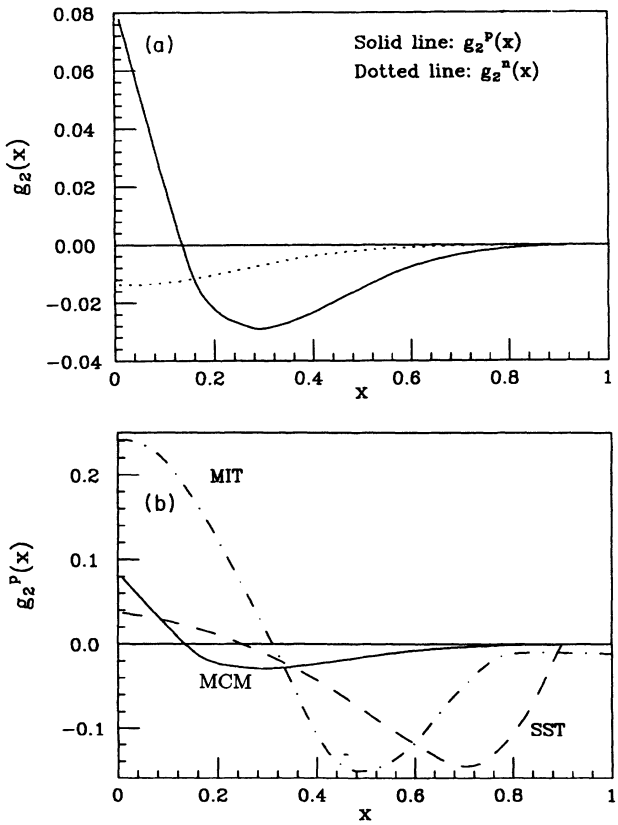

FIG. 11. (a) The calculated $g_2^p(x,Q^2)$ and $g_2^n(x,Q^2)$ given in this paper (valence contribution only). (b) Comparison of our $g_2^p(x,Q^2)$ (solid line) and those given by other models. Dot-dashed line: MIT bag model, dashed line: [40].

isfied. For SU(6) symmetry breaking wave function, $\int_0^1 g_2^p(x,Q^2)dx \simeq 0$; i.e., the BC sum rule is approximately satisfied. Similarly, $\int_0^1 g_2^n(x,Q^2)dx$ is also very small (10^{-3}) within the model. A comparison of $g_2^p(x)$ given by different models is shown in Fig. 11(b). The model dependence is easily seen, all models, however, give qualitatively similar results; i.e., $g_2(x)$ starts positive from $x \simeq 0$, changes its sign at some $x = x_0$ and after passing through a minimum it tends to zero. There are two distinctions between our result and those given by other models: (i) our g_2 is smaller than $(g_2)_{\rm MIT}$ and $(g_2)_{\rm SST}$ in the wide range of x and (ii) our x_0 ($\sim$0.15) is lower than $(x_0)_{\rm SST}$ ($\sim$0.25) and $(x_0)_{\rm MIT}$ ($\sim$0.30).

Unlike the unpolarized structure functions and g_1 of nucleon, the second spin structure function $g_2(x)$ involves contributions from the quark-gluon correlations and quark mass effects even in the large Q^2 limit. In the formalism of operator product expansion, these contributions come from local operators having twist 3. The structure function $g_2(x)$ can be decomposed into the two different twist pieces:

$$g_2(x) = g_2^{WW}(x) + \bar{g}_2(x), \tag{5.1}$$

where [70]

$$g_2^{WW}(x,Q^2) = -g_1(x,Q^2) + \int_x^1 dy g_1(y,Q^2)/y \tag{5.2}$$

is a twist-2 piece and

$$\bar{g}_2(x,Q^2) = g_1(x,Q^2) + g_2(x,Q^2) - \int_x^1 dy g_1(y,Q^2)/y \tag{5.3}$$

is the twist-3 piece. The model results of g_2^{WW} and $\bar{g}_2$ for the proton and neutron are shown in Figs. 12(a) and 12(b). Similar to other model calculations, our result also shows that although $g_2(x)$ is much smaller than $g_1(x)$, the twist-2 piece $g_2^{WW}(x)$ and twist-3 piece $\bar{g}_2(x)$ of the $g_2(x)$ are quite large, in particular in the small-x region. However, g_2^{WW} and $\bar{g}_2$ almost cancel, and the sum of them gives a very small g_2. So the higher twist effects cannot be neglected. Some numerical results are listed in Table III.

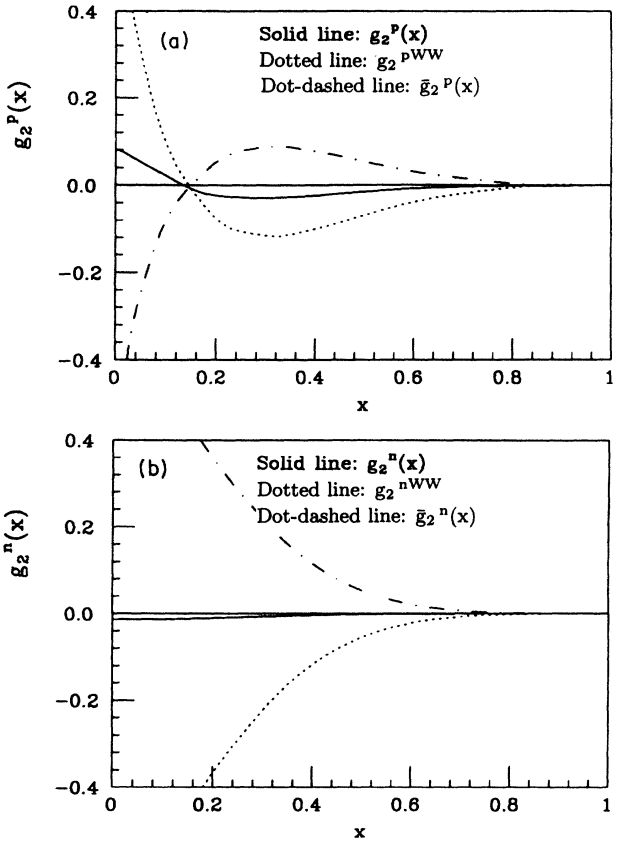

FIG. 12. (a) The calculated $g_2(x,Q^2)$ (solid line), $g_2^{WW}(x,Q^2)$ (dotted line), and $\bar{g}_2(x,Q^2)$ (dot-dashed line) for the proton. (b) Same as (a), but for the neutron.

VI. SUMMARY

In this paper both polarized and unpolarized structure functions for a free nucleon are calculated at moderate Q^2 value by using the modified c.m. bag model and evolved to higher Q^2 region by using leading-order perturbative QCD. Despite some approximations we have made, the model gives a reasonable description for the valence quark distributions at $x > 0.3$. For the small x region, the sea quark distributions are needed. For the unpolarized case, combining the valence and sea contri-

TABLE III. Comparison of the calculated moments of $g_1^{p,n}$ and $g_2^{p,n}$ given by different models with experiments.

Quantity	Data	MIT [34]	SST [40]	This paper
$\int[g_1^p(x)]_v dx$	–	0.175	0.220	0.1974
$\int[g_1^n(x)]_v dx$	–	0.0	–	0.0106
$\int[g_1^p(x)]_s dx$	–	0.0	–	−0.0714
$\int[g_1^n(x)]_s dx$	–	0.0	–	−0.0756
$\int g_1^p(x)dx$	0.126±0.018[a]	0.175	0.220	0.126
$\int g_1^n(x)dx$	−0.08±0.06[b]	0.0	–	−0.065
$\int[g_2^p(x)]_v dx$	–	0.0038	–	−0.0016
$\int[g_2^n(x)]_v dx$	–	–	–	−0.0047

[a]Data are taken from [12].
[b]Data are taken from [24].

butions, one can accommodate the existing unpolarized data except F_2^n/F_2^p at the large x region. The violation of the Gottfried sum rule can be attributed to a flavor asymmetric sea. For the spin-dependent structure functions, the existing data can be also accommodated within the model and a negatively polarized sea is required.

For unpolarized sea, the leading-order QCD evolution leads to a good or at least qualitative agreement with the data, if a moderate or very low Q_0^2 are used. On the other hand, the perturbative QCD is unable to give a negatively polarized sea, and various nonperturbative mechanisms should be further studied. In addition, it seems very likely that both the unpolarized and polarized seas violate SU(2) flavor symmetry. However, for the polarized sea, the uncertainties of model result and data are too large to make a definite conclusion.

The spin-dependent effect plays an important role in accommodating the data. In the model calculation, the magnitude and shape of u_v, d_v and Δu_v, Δd_v, in particular F_2^n/F_2^p, g_1^n and $g_2^{p,n}$ are sensitive to the symmetry-breaking effect which comes from spin-dependent interactions. Without the spin-dependent effect, we would obtain F_2^n/F_2^p=2/3, g_1^n=0, and $g_2^{p,n}$=0 if the sea contributions are ignored. Taking ξ=0.85, our result for F_2^n/F_2^p cannot accommodate the data in the large-x region. The possible sources which cause this failure presumably are (i) the cavity approximation for the quark wave function is too sharp at the boundary and does not have suitable "*soft*" behavior, and (ii) the parameter ξ which simulates the symmetry-breaking effects of the nucleon wave function is not good enough to describe different x behavior between u_v and d_v. Further studies on these problems are needed.

Finally, we note that only leading-order perturbative QCD evolution has been used. For the momentum transfer scale larger than $Q_0^2 \sim (0.9 - 1\ \mathrm{GeV}/c)^2$, we expect that perturbative next-to-leading-order QCD corrections and higher twist effects do not significantly change the leading-order result. However, it is well known that these corrections and higher-order effects become more and more important when x approaches the end points 0 and 1. Hence, our results are more reliable at the middle range of the x and less reliable at x near the end points.

ACKNOWLEDGMENTS

The authors acknowledge many useful conversations with H. J. Weber. We also thank P. K. Kabir, R. Lourie, O. Rondon-Aramayo, and other members of the INPP for their comments and suggestions. This work was supported by the U.S. Department of Energy and the Commonwealth Center for Nuclear and High Energy Physics, Virginia, USA.

APPENDIX A

We introduce the projection operators

$$\Lambda_{\mu\nu}^{(1)} = [-g_{\mu\nu} + \eta P_\mu P_\nu/M^2]/2\ ,$$
$$\Lambda_{\mu\nu}^{(2)} = \eta[-g_{\mu\nu} + 3\eta P_\mu P_\nu/M^2]/2 \qquad \text{(A1)}$$

which satisfy

$$\Lambda^{(1)\mu\nu} W_{\mu\nu} = W_1\ , \quad \Lambda^{(2)\mu\nu} W_{\mu\nu} = W_2. \qquad \text{(A2)}$$

Using (A2) and Eq. (2.11) in Sec. II, we obtain (3.1), where

$$I_{m_1}^{(1)}(l) = \Lambda^{(1)\mu\nu} I_{m_1,\mu\nu}(l)$$
$$= (1-\eta/2) I_{m_1}(l) + \eta I'_{m_1}(l) \qquad \text{(A3)}$$
$$I_{m_1}^{(2)}(l) = \Lambda^{(2)\mu\nu} I_{m_1,\mu\nu}(l)$$
$$= \eta[(1-3\eta/2) I_{m_1}(l) + 3\eta I'_{m_1}(l)] \qquad \text{(A4)}$$

where $\eta = 1/(1+\nu^2/Q^2)$, $l \equiv \mathbf{q} - \mathbf{k_1}$ and

$$I_{m_1}(l) = (2\pi)^3 \bar{\phi}_{m_1}(l) \not{k}_1 \phi_{m_1}(l) \qquad \text{(A5)}$$
$$I'_{m_1}(l) = (2\pi)^3 \bar{\phi}_{m_1}(l) \not{P} \phi_{m_1}(l)(k_1 P/M^2). \qquad \text{(A6)}$$

In the nucleon rest frame, $I_{m_1}(l) = I'_{m_1}(l)$; hence, we have

$$I_{m_1}^{(1)}(l) = (1+\eta/2) I_{m_1}(l), \qquad \text{(A7)}$$
$$I_{m_1}^{(2)}(l) = \eta(1+3\eta/2) I_{m_1}(l). \qquad \text{(A8)}$$

Until now we have not yet chosen the specific form of the rest frame quark wave function $q_m(\mathbf{r})$. To maintain the consistency, we use the same quark wave function as in [45], i.e., the cavity approximation

$$q_m(\mathbf{r}) = N(\omega)^{-1/2} \begin{pmatrix} i j_0(\omega r/R) U_m \\ -i j_1(\omega r/R) \vec{\sigma}\cdot\hat{\mathbf{r}} U_m \end{pmatrix} \qquad \text{(A9)}$$

and

$$\phi_m(\mathbf{k}) = (2/\pi)^{1/2} i R^3 [N(\omega)]^{-1/2} \begin{pmatrix} t_0(\omega, kR) U_m \\ t_1(\omega, kR) \vec{\sigma}\cdot\hat{\mathbf{k}} U_m \end{pmatrix}, \qquad \text{(A10)}$$

where $t_i(\alpha,\beta) = \int_0^1 x^2 dx j_i(\alpha x) j_i(\beta x)$ (i=0,1), ω =2.04, $\hat{\mathbf{k}} = \mathbf{k}/|\mathbf{k}|$, R is the bag radius. The normalization factor is $N(\omega) = 4\pi R^3[1 - j_0^2(\omega)]/\omega^2$. Using (A10), the spectator quark pieces (2.11) can be rewritten as

$$I_{m_j}(\mathbf{k_j}) = C_j 2k_j [t_0(\omega, k_j R_j) + t_1(\omega, k_j R_j)]^2 \qquad (j = 2,3) \qquad \text{(A11)}$$

and the struck quark pieces (A7) and (A8) become

$$I_{m_1}^{(1)}(\mathbf{k_1} - \mathbf{q}) = C_1(1+\eta/2) 2k_1 [t_0^2(\omega, lR_1) + t_1^2(\omega, lR_1)] \qquad \text{(A12)}$$
$$I_{m_1}^{(2)}(\mathbf{k_1} - \mathbf{q}) = C_1 \eta(1+3\eta/2) \times 2k_1 [t_0^2(\omega, lR_1) + t_1^2(\omega, lR_1)] \qquad \text{(A13)}$$

where $C_i = 8\pi^2 R_i^6/N(\omega)$ (i=1,2,3). For brevity, we define the dimensionless variables: $\beta_i \equiv k_i R_1$ (i=1,2), $\beta_0 \equiv l_0 R_1 = |\ (M+q_0)R_1 - \beta_1\ |$, $\beta_3 \equiv \beta_0 - \beta_2$, $\beta \equiv |\ \mathbf{q} - \mathbf{k_1}\ | R_1$, $\delta \equiv |\ \mathbf{q}\ | R_1$ and $\epsilon = (\mathbf{p_1})_{\max} R_1$ where $(\mathbf{p_1})_{\max}$ is the maximum value of three momentum of the struck quark inside the nucleon. Using these variables, we have

$$\int d^3\mathbf{k}_2 d^3\mathbf{k}_3 \delta^4\left(q+p-\sum_i \mathbf{k}_i\right) \to 2\pi/(\beta R^2)\int_{(\beta_0-\beta)/2}^{(\beta_0+\beta)/2} d\beta_2\beta_2(\beta_2-\beta_0) \quad \text{(A14)}$$

and

$$\int d^3\mathbf{k}_1 \to (2\pi/\delta)\int_{\delta-\epsilon}^{\delta+\epsilon}\beta_1 d\beta_1 \int_0^{\beta_0} \beta d\beta. \quad \text{(A15)}$$

Substituting (A11) and (A12) into (3.1), using (A14) and (A15) we finally obtain

$$W_1(x,Q^2) = N(1+\eta/2)\sum_{1\to 2,3}\sum_{\alpha} b_\alpha(1;23)C(1;23)I_\alpha(R_1;\xi_2,\xi_3) \quad \text{(A16)}$$

i.e., (3.2), where

$$I_\alpha(R_1;\xi_2,\xi_3) = \int_{\delta-\epsilon}^{\delta+\epsilon}\beta_1 d\beta_1 \int_0^{\beta_0}(\beta/\delta)d\beta[t_0^2(\omega,\beta)+t_1^2(\omega,\beta)]I_\alpha^{(23)}(\beta_0,\beta) \quad \text{(A17)}$$

and

$$I_\alpha^{(23)}(\beta_0,\beta) = \int_{(\beta_0-\beta)/2}^{(\beta_0+\beta)/2}(\beta_2/\beta)(\beta_2-\beta_0)d\beta_2\prod_{i=2}^{3}[t_0(\omega,\xi_i\beta_i)+t_1(\omega,\xi_i\beta_i)]^2, \quad \text{(A18)}$$

where $t_i(a,b) = \int_0^1 x^2 dx j_i(ax)j_i(bx)$ $(i=0,1)$ and $\omega = 2.04$. Similarly, we can obtain (3.3).

We note that although the quark wave function (A9), or (A10), has been used, other options are allowed. For instance, a Gaussian-type wave function [71]

$$q_m(\mathbf{r}_i) = (\alpha/\sqrt{\pi})^{1/2}e^{\alpha^2R^2/2}\begin{pmatrix} U_m \\ i(\alpha^2/2m_q)\vec{\sigma}\cdot\vec{\mathbf{r}}_i U_m\end{pmatrix}e^{-\alpha^2 r_i^2/2} \quad \text{(A19)}$$

and its Fourier transformation

$$\phi_m(\mathbf{k}_i) = 1/(\alpha^2\sqrt{\pi})e^{\alpha^2R^2/2}\begin{pmatrix} U_m \\ (1/2m_q)\vec{\sigma}\cdot\vec{\mathbf{k}}_i U_m\end{pmatrix}e^{-p_i^2/2\alpha^2} \quad \text{(A20)}$$

can be used to calculate the structure functions.

In the Bjorken limit, $\nu/|\mathbf{q}| \to 1$, $\eta \to 0$ and $|\mathbf{q}| \simeq q_0 + Mx$, then $\beta_0 = (M+q_0-|\mathbf{q}|)R_1 \to MR_1(1-x)$, hence the integral $\int_0^{\beta_0}\beta d\beta[t_0^2(\omega,\beta)+t_1^2(\omega,\beta)]I_\alpha^{(23)}(\beta_0,\beta)$ depends only on x. Considering that the initial quark momentum is much smaller than the virtual photon momentum, i.e., $|\mathbf{p}_1| \ll |\mathbf{q}|$, therefore $\epsilon \ll \delta$, one can see that the β_1 value is restricted in a very narrow region around δ: $\delta \pm \epsilon$, and the integral over β_1 can be approximately given by the mean-value theorem. Then (A17) becomes

$$I_\alpha(R_1;\xi_2,\xi_3) \simeq 2\epsilon\int_0^{\beta_0}\beta d\beta[t_0^2(\omega,\beta)+t_1^2(\omega,\beta)]I_\alpha^{(23)}(\beta_0,\beta) \quad \text{(A21)}$$

which depends only on the variable x; hence, both $F_1(x)$ and $F_2(x)$ are scaling in the Bjorken limit and vanish when $x \to 1$. Numerical calculations also confirm this conclusion.

APPENDIX B

From (2.9) and (2.12), we have

$$W_{\mu\nu}^{(A)}(P,q,S) = \epsilon_{\mu\nu\lambda\sigma}k_1^\lambda \sum_{1\to 2,3}\sum_{\alpha_1,m_1} b_{\alpha_1,m_1}(1;23)M(4\pi^2R_1)^{-3}\int\prod_{i=1}^{3} d^3\mathbf{k}_i/(2k_i) \times\delta^4(q+P-\sum_i k_i)I_{m_1}^{(A)\sigma}(\mathbf{k}_1-\mathbf{q})I_{m_2}(\mathbf{k}_2)I_{m_3}(\mathbf{k}_3) \quad \text{(B1)}$$

where the axial-vector current piece coming from the struck quark $I_{m_1}^{(A)\sigma}(\mathbf{k}_1-\mathbf{q})$ has been given in (4.3). Using (A10),

it is easy to show that

$$\bar{\phi}_m(\mathbf{k}_1-\mathbf{q})\gamma^\sigma\gamma^5\phi_m(\mathbf{k}_1-\mathbf{q}) = (2/\pi)(R_1^6/N)\mathrm{sgn}(m)\begin{cases} -2(\beta_z/\beta)t_0t_1, & \sigma=0 \\ t_0^2+(2\beta_z^2/\beta^2-1)t_1^2, & \sigma=3 \end{cases} \tag{B2}$$

where $\beta_z = |(\mathbf{q}-\mathbf{k}_1)_z|R_1$.

Substituting (B2) and the spectator quark pieces (A11) into (B1) and using (A14) and (A15), we arrive at (4.6). The results for $I_L^{0,3}$, I_T^3, and g_1, g_2 are listed below.

(i) For $\mathbf{q} \parallel -\mathbf{S}$:

$$I_L^i = N\pi \sum_{1\to 2,3}\sum_{\alpha_1,m_1} b_{\alpha_1,m_1}(1;23)C(1;23)\mathrm{sgn}(m_1)I_L^{(i)}(\beta_0,\delta,\epsilon) \quad (i=0,3) \tag{B3}$$

with

$$I_L^{(0)}(\beta_0,\delta,\epsilon) = \int_{\delta-\epsilon}^{\delta+\epsilon} d\beta_1 \int_0^{\beta_0} d\beta(-2\beta_z)t_0(\omega,\beta)t_1(\omega,\beta)I_{\alpha_1}^{(23)}(\beta_0,\beta) \tag{B4}$$

and

$$I_L^{(3)}(\beta_0,\delta,\epsilon) = \int_{\delta-\epsilon}^{\delta+\epsilon} d\beta_1 \int_0^{\beta_0} \beta d\beta[t_0^2(\omega,\beta)+(2\beta_z^2/\beta^2-1)t_1^2(\omega,\beta)]I_{\alpha_1}^{(23)}(\beta_0,\beta), \tag{B5}$$

where $\beta_z = (\beta_1^2-\delta^2-\beta^2)/2\delta$ and the spectator quark contribution $I_\alpha^{(23)}(\beta_0,\beta)$ is the same as that in the unpolarized case, i.e., (A18).

It can be shown

$$g_1 = (1-\eta)[I_L^3 + I_L^0/\sqrt{1-\eta} + I_T^3\eta/(1-\eta)]. \tag{B6}$$

In the Bjorken limit, (B6) reduces into (4.4).

(ii) For $\mathbf{q} \perp \mathbf{S}$:

$$I_T^3 = N\pi \sum_{1\to 2,3}\sum_{\alpha_1,m_1} b_{\alpha_1,m_1}(1;23)C(1;23)\mathrm{sgn}(m_1)I_T^{(3)}(\beta_0,\delta,\epsilon) \tag{B7}$$

where

$$I_T^{(3)}(\beta_0,\delta,\epsilon) = \int_{\delta-\epsilon}^{\delta+\epsilon} d\beta_1 \int_0^{\beta_0} d\beta\{t_0^2(\omega,\beta)+[(\beta_1^2-\beta_{1x}^2)/\beta^2-1]t_1^2(\omega,\beta)\}I_\alpha^{(23)}(\beta_0,\beta), \tag{B8}$$

where $\beta_{1x} = (\beta^2-\delta^2-\beta_1^2)/2\delta$. Similarly, we have

$$g_2 = (1-\eta)[I_T^3 - I_L^3 - I_L^0/\sqrt{1-\eta}] \tag{B9}$$

which, combining (B6), reduces into (4.5) in the Bjorken limit.

[1] T. Sloan, G. Smadja, and R. Voss, Phys. Rep. **162**, 45 (1988).
[2] S. R. Mishra and F. Sciulli, Annu. Rev. Nucl. Part. Sci. **39**, 259 (1989).
[3] R. G. Roberts and M. R. Whalley, J. Phys. G **17**, D1 (1991).
[4] J. F. Owens and W. K. Tung, Ann. Rev. Nucl. Part. Sci. **42**, 291 (1992).
[5] A. Milsztajn *et al.*, Z. Phys. C **49**, 527 (1991).
[6] P. Amaudruz *et al.*, Phys. Rev. Lett. **66**, 2712 (1991).
[7] K. Gottfried, Phys. Rev. Lett. **18**, 1174 (1967).
[8] H. Abramowicz *et al.*, Z. Phys. **C15**, 19 (1982).
[9] C. Foudas *et al.*, Phys. Rev. Lett. **64** 1207 (1990).
[10] M. J. Alguard *et al.*, Phys. Rev. Lett. **37**, 1261 (1976); **41**, 70 (1978).
[11] G. Baum *et al.*, Phys. Rev. Lett. **45**, 2000 (1980); **51**, 1135 (1983).
[12] J. Ashman *et al.*, Phys. Lett. B **206**, 364 (1988); Nucl. Phys. **B328**, 1 (1989).
[13] V. W. Hughes and J. Kuti, Ann. Rev. Nucl. Part. Sci. **33**, 611 (1983).
[14] J. Ellis and R. L. Jaffe, Phys. Rev. D **9**, 1444 (1974); **10**, 1669 (1974).
[15] J. D. Bjorken, Phys. Rev. **148**, 1467 (1966); Phys. Rev. D **1**, 1376 (1970).
[16] SMC Collaboration, B. Adeva *et al.*, Phys. Lett. B **302**, 534 (1993); **320**, 400 (1994).
[17] E. Henley, Bull. Am. Phys. Soc. **38**, 972 (1993); D. L. Anthony *et al.*, Phys. Rev. Lett. **71**, 959 (1993).
[18] J. Ellis and M. Karliner, Phys. Lett. B **313**, 131 (1993).
[19] S. J. Brodsky, J. Ellis, and M. Karliner, Phys. Lett. B **206**, 309 (1988).
[20] G. Altarelli and G. G. Ross, Phys. Lett. B **212**, 391 (1988).
[21] R. D. Carlitz, J. C. Collins, and A. H. Mueller, Phys. Lett. B **214**, 229 (1988).

[22] A. V. Efremov and O. V. Teryaev, Dubna Report No. E2-88-287 [Czech. Hadron Symp. 302 (1988).
[23] G. Altarelli and W. J. Stirling, Particle World, **1**, 40 (1989).
[24] R. L. Jaffe and A. Manohar, Nucl. Phys. **B337**, 509 (1990).
[25] E. Reya, Dortmund Report No. DO-TH 91/09 (unpublished).
[26] K. A. Griffioen, in *CEBAF 1992 Summer Workshop*, Newport News, Virginia, 1992, edited by Franz Gross and Roy Holt, AIP Conference Proc. No. 269 (AIP, New York, 1992), p. 271.
[27] A. Ukawa, in *Lattice '92*, Proceedings of the International Symposium, Amsterdam, The Netherlands, 1992, edited by J. Smit and P. van Baal [Nucl. Phys. B (Proc. Suppl.) **30**, 3 (1993)].
[28] R. Altmeyer, M. Gockeler, R. Horsley, E. Laermann, and G. Schierholz, in *Lattice '92* [27], p. 483.
[29] S. J. Dong and Keh-Fei Liu, in *Lattice '92* [27], p. 487.
[30] R. L. Jaffe, Phys. Rev. D **11**, 1953 (1975).
[31] R. J. Hughes, Phys. Rev. D **16**, 622 (1977); J. A. Bartelski, *ibid.* **20**, 1229 (1979).
[32] J. S. Bell and A. J. G. Hey, Phys. Lett. **74B**, 77 (1978); J. S. Bell, A. C. Davis, and J. Rafelski, *ibid.* **78B**, 67 (1978).
[33] L. S. Celenza and C. M. Shakin, Phys. Rev. C **27**, 1561 (1983); C **39**, 2477 (E) (1989).
[34] R. L. Jaffe and Xiangdong Ji, Phys. Rev. D **43**, 726 (1991).
[35] X. M. Wang, X. Song, and P. C. Yin, Hadron J., **6**, 985 (1983); X. M. Wang, Phys. Lett. **140B**, 413 (1984).
[36] C. J. Benesh and G. A. Miller, Phys. Rev. D **36**, 1344 (1987); **38**, 48 (1988).
[37] R. E. Peierls and J. Yoccoz, Proc. Phys. Soc. A **70**, 381 (1957); R. E. Peierls and D. J. Thouless, Nucl. Phys. **38**, 154 (1962).
[38] A. De Rújula, H. Georgi, and S. L. Glashow, Phys. Rev. D **12**, 147 (1975)
[39] H. Meyer and P. J. Mulders, Nucl. Phys. **A528**, 589 (1991).
[40] A. W. Schreiber, A. I. Signal, and A. W. Thomas, Phys. Rev. D **44**, 2653 (1991).
[41] M. R. Bate and A. I. Signal, J. Phys. G **18**, 1875 (1992).
[42] R. P. Bickerstaff and J. L. Londergan, Phys. Rev. **42**, 3621 (1990).
[43] M. Traini, L. Conci, and U. Moschella, U. Trento-Louvain report, 1992 (unpublished).
[44] N. Isgur and G. Karl, Phys. Rev. D **18**, 4187 (1978); **20**, 2653 (1979).
[45] X. Song and J. S. McCarthy, Phys. Rev. C **46**, 1077 (1992).
[46] G. Altarelli and G. Parisi, Nucl. Phys. **B126**, 298 (1977).
[47] Q. Shen, C. Wu, J. Lu, and P. Zhao, Physica Energiae Fortis et Physica Nuclearis **7**, 170 (1983).
[48] X. Song and J. Du, Phys. Rev. D **40**, 2177 (1989).
[49] H. Burkhardt and W. N. Cottingham, Ann. Phys. (N. Y.) **56**, 453 (1970).
[50] R. P. Feynman and R. D. Field, Phys. Rev. D **15**, 2590 (1977).
[51] D. A. Ross and C. T. Sachrajda, Nucl. Phys. **B149**, 497 (1979).
[52] J. F. Donoghue and E. Golowich, Phys. Rev. **D15**, 3421 (1977).
[53] H. He, X. Zhang, and Y. Zhuo, Chinese Phys. **4**, 365 (1984).
[54] J. D. Sullivan, Phys. Rev. D **5**, 1732 (1972)
[55] E. M. Henley and G. A. Miller, Phys. Lett. B **251**, 453 (1990).
[56] J. Stern and G. Clement, Phys. Lett. B **264**, 426 (1991).
[57] A. Signal, A. W. Schreiber, and A. W. Thomas, Mod. Phys. Lett. **A6**, 271 (1991).
[58] S. Kumano and J. T. Londergan, Phys. Rev. D **44**, 717 (1991).
[59] A. Anselmino, V. Barone, F. Caruso, and E. Predazzi, Z. Phys. C **55**, 97 (1992).
[60] X. Song and H. J. Weber, Report No. INPP-UVA-92-17 (unpublished).
[61] E. V. Schuryak and J. L. Rosner, Phys. Lett. B **218**, 72 (1989), and references therein.
[62] H. J. Weber, Phys. Rev. D (to be published).
[63] R. P. Feynman, *Photon-Hadron Interactions* (W. A. Benjamin, New York, 1972).
[64] L. Ahrens *et al.*, Phys. Rev. D **35**, 785 (1987).
[65] F. E. Close, Nucl. Phys. **A508**, 413 (1990).
[66] P. G. Ratcliffe, Phys. Lett. B **192**, 180 (1987).
[67] H. Y. Cheng and C. F. Wai, Phys. Rev. D **46**, 125 (1992).
[68] S. Y. Hsueh *et al.*, Phys. Rev. D **38**, 2056 (1988).
[69] A. E. Dorokhov and N. I. Kochlev, Mod. Phys. Lett. A **5**, 55 (1990).
[70] S. Wandzura and F. Wilczek, Phys. Lett. **82B**, 195 (1977).
[71] M. Beyer and H. J. Weber, Phys. Rev. C **35**, 14 (1987).
[72] Particle Data Group, K. Hikasa *et al.* Phys. Rev. D **45**, S1 (1992).
[73] F. E. Close and R. G. Roberts, Report No. RAL-93-040 (unpublished).